

**Excitation and propagation of surface polaritonic rogue waves and breathers**

Saeid Asgarnezhad-Zorgabad and Rasoul Sadighi-Bonabi\*

*Department of Physics, Sharif University of Technology, Azadi Avenue, Tehran, Iran*

Barry C. Sanders†

*Institute for Quantum Science and Technology, University of Calgary, Alberta, Canada T2N 1N4;**Program in Quantum Information Science, Canadian Institute for Advanced Research, Toronto, Ontario, Canada M5G 1M1;**and Light and Matter Physics Group, Raman Research Institute, Bangalore 560080, India*

(Received 26 February 2018; published 13 July 2018)

Excitation and propagation of the surface polaritonic rogue waves and breathers are investigated by proposing a coupler free optical waveguide that consists of a transparent layer, middle negative index metamaterial layer, and bottom layer of the cold four level atomic medium. In this planar optical waveguide, a giant controllable Kerr nonlinearity is achieved by sufficient field concentration and a proper set of intensities and detunings of the driven laser fields. As a result, various kinds of temporal surface polaritonic solitons, rogue waves, and breathers can be propagated in the narrow window for electromagnetically induced transparency. We find that the giant intensity and extreme concentration of surface polaritons with low generation power can be achieved by excitation of the first- and second-order peregrine rogue waves. Furthermore, the first- and higher-order surface polaritonic Akhmediev breathers can be propagated at the slow light level due to modulation instability in the proposed optical waveguide. We demonstrate that surface-polariton propagation length can be significantly enhanced by Kuznetsov-Ma breather dynamics.

DOI: [10.1103/PhysRevA.98.013825](https://doi.org/10.1103/PhysRevA.98.013825)**I. INTRODUCTION**

Rogue waves are low-probability, high-amplitude events that can arise in the dynamical behavior of a particular system [1–3]. The dramatic impact and nature of these waves are widely studied [4,5]. In the past few decades, experiments have been proposed to demonstrate existence of rogue waves and breathers in various physical systems such as water waves [6], optical fibers, optical cavities [7], photorefractive crystals [8], Bose-Einstein condensates [9], plasmas [10], and laser-induced dielectric filamentation [11]. Moreover, various theoretical investigations such as standard self-focusing nonlinear Schrödinger equations (NLSEs), higher-order NLSEs [12], the Hirota equation [13], the Sasa-Satsuma equation [14], and the Davey-Stewartson equation [15] have been developed in order to investigate the conditions where the rogue waves and breathers (i.e., peregrine, Akhmediev, and Kuznetsov-Ma breathers) can form [16,17].

During the past decade, observing nonlinear waves (e.g., solitons, rogue waves, and breathers) in optics has become of paramount importance due to their potential applications to supercontinuum generation [18], pulsed operation of mode-locked lasers [19,20], photonic-crystal fibers [21], Raman amplifiers [22], parametric processes [23], spatiotemporal structures [24], and more [25,26]. Among these phenomena, optical rogue waves have been observed in whispering-gallery-mode resonators as a result of chaotic interplay between

the Kerr nonlinearity and group-velocity dispersion (GVD) [27]. Alongside these investigations, elementary breathers and higher-order solitons on finite background structures can be observed by chaotic modulation instability. Dynamical behavior of these waves can be described by the NLSE; as a result, various rogue waves can be effectively identified by means of solitons on finite background collisions [28]. Recently, resonant interaction of two-level ion with an optical field has shown that the optical field component has peregrinelike structure, whereas the matter wave experiences more complicated, yet spatiotemporal-balanced, amplitude distribution [29].

The peregrine soliton has been observed in the semiclassical limit of the NLSE [30] by nonlinear propagation of the intense laser pulse into the optical fiber. The optical Kerr nonlinearity in a typical optical fiber is typically weak and as a result the observation of rogue waves and breathers need the high input power [31]. Very recently, the weak nonlinearity and necessity of the high optical field input power have been overcome by considering the cold three-level electromagnetically induced transparency (EIT) sample as a potential nonlinear medium. In this work the rogue waves and different types of breathers are also observed at the weak light level [32].

The mentioned investigations indicate that the dynamics of the optical rogue waves and breathers in the self-focusing medium can be described by the NLSE. On the other hand, many theoretical and experimental proposals demonstrate that the combination of a dielectric medium with a negative-index metamaterial (NIMM) optical waveguide is a nonlinear system and stable linear and nonlinear surface polaritons (SPs) can be propagated through NIMM-dielectric interface by doping thin multilevel atomic medium as a substrate [33–36]. Therefore, a

\*sadighi@sharif.edu

†sandersb@ucalgary.ca; <http://iqst.ca/people/peoplepage.php?id=4>

natural question that appears is whether the surface polaritonic rogue waves and breathers can be excited and propagated in the experimentally feasible scheme. To the best of our knowledge, the propagation and excitation of the surface polaritonic rogue waves and breathers has not been investigated.

We propose a planar polaritonic waveguide comprising an upper transparent medium, a middle NIMM layer, and a bottom layer containing a four-level cold  $N$ -type atomic medium [37]. Our results show that stable and efficient propagation of the polaritonic rogue waves and breathers can be achieved by controlling the linear and nonlinear optical properties of SPs at weak light level. In the linear regime, the large-field concentration, i.e.,

$$|E_{nd}|^2 \approx 6|E_0|^2, \quad (1)$$

reduced reflection, and the modulated dielectric constant of the atomic ensemble are obtained in the narrow EIT window and as a result the SPs can be excited without the dielectric coupler.

The existence of mode confinement and suitable adjustment of the driven laser intensities and detunings results in the controllable Kerr nonlinearity–group-velocity dispersion couples which makes it possible to excite various types of (1 + 1)-dimension [i.e., (1 + 1)D; one dimension depicted position and one dimension for time variation] surface polaritonic solitons. This efficient SP excitation and giant self-focusing, self-defocusing nonlinearity then lead to surface polaritonic rogue waves and breathers propagation. It is noticed that the first- and higher-order surface polaritonic peregrine breather can be explicitly achieved in our proposed scheme. Moreover, the MI results in the formation and evolution of the different orders of the Akhmediev breathers.

We show that the intense surface polaritonic train with sufficiently enhanced propagation length can be propagated by Kuznetsov-Ma breathers in this polaritonic waveguide. Our results have two main aspects.

(i) High-amplitude and extreme concentration of SP rogue waves achieved by excitation of first- and second-order peregrine rogue wave as well as two-mode Akhmediev breather collisions that may have applications in plasmonics [38].

(ii) Formation of various SP breathers with sufficiently large intensity results in the enhancement of the SP's propagation length, which is suitable for optical communication devices.

## II. MODEL

Excitation and propagation of the surface polaritonic rogue waves and breathers can be investigated by proposing a coupler-free optical waveguide as shown in Fig. 1. This polaritonic device consists of three layers. The upper layer is supposed to be a transparent layer with

$$n_t = \sqrt{\frac{\varepsilon_t \mu_t}{\varepsilon_0 \mu_0}} \approx 1. \quad (2)$$

$\varepsilon_t$  and  $\mu_t$  are the electrical permittivity and magnet permeability of the upper layer, NIMM is superposed as a middle layer, and a coherently driven cold four-level  $N$ -type atomic medium is considered as a bottom medium of the waveguide. The optical properties of the NIMM layer can be described by

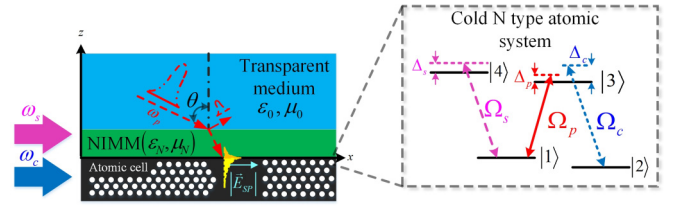


FIG. 1. Free space coupled planar waveguide: the surface polaritons can be excited and propagated through the  $x$  axis in the NIMM–quantum emitter interface [39]. The system consists of transparent medium (the optical properties of this medium  $\varepsilon_t$  and  $\mu_t$ ), middle layer of NIMM (with electrical permittivity  $\varepsilon_N$  and magnetic permeability  $\mu_N$ ), and coherently driven cold four-level  $N$  type atomic medium is set as a quantum emitter in the bottom layer (the white dots). The inset of the figure denotes the cold atomic medium with energy-level diagram.  $\omega_l$ ;  $l \in \{c, p, s\}$  are the center frequencies of the couple, probe, and signal laser fields,  $|l\rangle$  is the bare atomic state, and  $\Delta_l$  are corresponded detunings (see the text for details).

the simple Drude model, i.e.,

$$\begin{aligned} \varepsilon_N(\omega_l) &= \varepsilon_\infty - \frac{\omega_e^2}{[\omega_l(\omega_l + i\gamma_e)]}, \\ \mu_N(\omega_l) &= \mu_\infty - \frac{\omega_m^2}{[\omega_l(\omega_l + i\gamma_m)]}, \end{aligned} \quad (3)$$

where  $\varepsilon_\infty(\mu_\infty)$  is the background constant of permittivity (permeability),  $\omega_l$  is the oscillation frequency,  $\omega_e(\omega_m)$  is the electric (magnetic) plasma frequency, and  $\gamma_e(\gamma_m)$  is the corresponding decay rate). Moreover, the quantum emitters are supposed to be a four-level cold  $N$ -type atomic medium. This sample is then cooled with the magneto-optical trap (MOT) technique and embedded to the bottom of the NIMM layer as a thin substrate.

This cold atomic layer with energy levels

$$E_j = \hbar\omega_j \quad (4)$$

and atomic transition  $|j\rangle$  ( $j \in \{1, 2, 3, 4\}$ ) are then pumped by the three laser fields  $\omega_l$  ( $l \in \{c, s, p\}$ ) in which the couple, probe, and signal laser are coupled the  $|2\rangle \rightarrow |3\rangle$ ,  $|1\rangle \rightarrow |3\rangle$ , and  $|1\rangle \rightarrow |4\rangle$ , respectively, with the corresponding detunings

$$\begin{aligned} \Delta_c &= \omega_c - \omega_{23}, \\ \Delta_p &= \omega_p - \omega_{13}, \\ \Delta_s &= \omega_s - \omega_{14}. \end{aligned} \quad (5)$$

The total electric-field vector of the medium is

$$\mathbf{E}(\mathbf{r}, t) = \sum_{l=c, s, p} \mathbf{E}_l(\mathbf{r}, t) + \text{c.c.}, \quad (6)$$

with

$$\mathbf{E}_l(\mathbf{r}, t) = \mathcal{E}_l \mathbf{u}_l(\mathbf{r}) e^{i(\mathbf{k}_l \cdot \mathbf{r} - \omega_l t)} \quad (7)$$

and

$$\mathcal{E}_l = \left( \frac{\hbar\omega_l}{\varepsilon_0 L_x L_y L_z} \right)^{1/2} \hat{a}(\omega_l) \quad (8)$$

being the amplitude of the electric mode component,  $L_{x(y)}$  the length of the NIMM–cold gas interface in the  $x(y)$  directions,

$\hat{a}(\hat{a}^\dagger)$  the creation (annihilation) operator of the quantized electric field, and

$$L_z = \sum_{j=n,t} \left\{ \left( \frac{\omega_j^2}{2c^2} \right) \left[ \frac{\tilde{\varepsilon}_j(|k|^2 + |k_j|^2)}{|k_j|\varepsilon_j^2} \right] + \frac{\tilde{\mu}_j}{2|k_j|} \right\}, \quad (9)$$

with

$$\tilde{\varepsilon}_j \equiv \text{Re} \left[ \frac{\partial(\omega_j \varepsilon_1)}{\partial \omega_1} \right], \quad \tilde{\mu}_j \equiv \text{Re} \left[ \frac{\partial(\omega_j \mu_1)}{\partial \omega_1} \right] \quad (10)$$

being the effective mode length that determines the confinement of the EM mode at the interface and

$$\mathbf{u}_1(\mathbf{r}) = c[k(\omega_1)\mathbf{e}_z - ik_l(\omega_1)\mathbf{e}_x]e^{k_l(\omega_1)r}/\varepsilon_l\omega_1. \quad (11)$$

The Hamiltonian of the proposed cold atomic medium in the interaction picture and under the rotating-wave and dipole approximations is

$$\mathcal{H}_I = \hbar \left[ \sum_{l=1}^4 \Delta_l |l\rangle \langle l| + \zeta_c(z)\Omega_c |3\rangle \langle 2| + \zeta_p(z)\Omega_p |3\rangle \langle 1| + \zeta_s(z)\Omega_s |4\rangle \langle 1| + \text{c.c.} \right], \quad (12)$$

where  $\Delta_1 = 0$  and

$$\begin{aligned} \Delta_2 &= \omega_p - \omega_c + \frac{E_1 - E_2}{\hbar}, \\ \Delta_3 &= \omega_p - \frac{E_3 - E_1}{\hbar}, \\ \Delta_4 &= \omega_s - \frac{E_4 - E_1}{\hbar}. \end{aligned} \quad (13)$$

Moreover, one can assume  $\omega_c \approx \omega_p \approx \omega_s$ . Therefore, we have

$$\zeta_c(z) \approx \zeta_p \approx \zeta_s \approx \mathbf{e}_{13} \cdot \mathbf{u}_p(z). \quad (14)$$

Here  $\mathbf{e}_{ij}$  is the atomic electrical dipole moment of the  $|i\rangle \rightarrow |j\rangle$  transition (i.e.,  $\mathbf{p}_{ij} = \mathbf{e}_{ij}|p_{ij}|$ ).

The quantities

$$\Omega_c = |\mathbf{p}_{23}| \mathcal{E}_c / \hbar, \quad \Omega_p = |\mathbf{p}_{13}| \mathcal{E}_p / \hbar, \quad \Omega_s = |\mathbf{p}_{14}| \mathcal{E}_s / \hbar \quad (15)$$

are the half-Rabi frequency of the couple, probe, and signal fields, respectively. The dynamics of the atomic medium is given by the Bloch equation

$$i\hbar \left( \frac{\partial}{\partial t} + \Gamma \right) \tilde{\rho} = [\mathcal{H}_I, \tilde{\rho}], \quad (16)$$

with  $\Gamma$  the  $4 \times 4$  matrix describing the decay rates of the cold atomic medium. Explicit solutions of the Bloch equations is presented in Appendix A.

Here we take advantage of the coupler free scheme, as this design is experimentally feasible [40]. As shown in Sec. III this waveguide is suitable for coherent excitation of the SP mode. For efficient excitation, the field enhancement in the NIMM–cold atoms interface should be greatly enhanced and the transmittance  $T$  and total reflection  $R$  should be modulated as  $T \gg R$ . To achieve this, the three-layer reflection coefficient in the proposed scheme can be expressed as [41]

$$r_{\text{nd}} = \frac{r_{\text{tn}} + r_{\text{nd}} e^{ik_{\text{nx}}l}}{1 + r_{\text{tn}} r_{\text{nd}} e^{2ik_{\text{nx}}l}}, \quad (17)$$

where

$$r_{\text{tn}} = \frac{\varepsilon_N k_{\text{tx}} - \varepsilon_t k_{\text{Nx}}}{\varepsilon_N k_{\text{tx}} + \varepsilon_t k_{\text{Nx}}}, \quad r_{\text{nd}} = \frac{\varepsilon_d k_{\text{Nx}} - \varepsilon_N k_{\text{dx}}}{\varepsilon_d k_{\text{Nx}} + \varepsilon_N k_{\text{dx}}} \quad (18)$$

is the reflection coefficient of the transparent-NIMM and NIMM–atomic-medium interface, respectively,

$$k_{lx}^2 = k_z^2 - \frac{\omega^2 \varepsilon_1 \mu_1}{c^2} \quad (19)$$

with ( $k_z = k_0 n_l \sin \theta$ ,  $l \in \{t, N, d\}$ ) being the normal component of the electrical field in the  $l$ th medium with  $k_0 = 2\pi/\lambda_p$ ,  $\lambda_p$  the wavelength of the probe laser field,  $\theta$  the angle of incidence, and  $\varepsilon_d$  the dielectric constant of the atomic medium, which is given by the following expression [42]:

$$\varepsilon_d = 1 + \frac{\chi_p}{1 - \chi_p/3}, \quad (20)$$

where  $\chi_p$  is the yet to be determined susceptibility of the atomic medium, which is expanded into different orders of perturbation.

Excitation of the SP modes can then be obtained by the field enhancement in the atomic medium–NIMM interface and special modulation of the dielectric constant of the atomic sample. On the other hand, the Maxwell equation is used for the control of the weak probe field in this planar waveguide, i.e.,

$$\nabla^2 \mathbf{E}_p - \left( \frac{1}{c^2} \right) \frac{\partial^2 \mathbf{E}_p}{\partial t^2} = \frac{1}{\varepsilon_0 c^2} \frac{\partial^2 \mathbf{P}_p}{\partial t^2}, \quad (21)$$

with

$$\mathbf{P}_p = N_a \mathbf{p}_{31} \tilde{\rho}_{31} e^{i(\mathbf{k}_p \cdot \mathbf{r} - \omega_p t)} \quad (22)$$

treated as the probe-field polarization intensity.

Using the slowly varying amplitude approximation [ $|\partial^2 \Omega_p / \partial x^2| \ll |2ik_p(\partial \Omega_p / \partial z)|$ ] the Maxwell equation reduces to the expression

$$i \left( \frac{\partial}{\partial x_0} + \frac{1}{n_{\text{eff}} c} \frac{\partial}{\partial t_0} \right) \Omega_p + \kappa_{13} \langle \tilde{\rho}_{13} \rangle = 0, \quad (23)$$

where  $\kappa_{13} = N_a \omega_p |\hat{\mathbf{e}}_p \cdot \mathbf{p}_{13}|^2 / 2\hbar \varepsilon_0 c$ ,  $N_a$  is the atomic density,  $\omega_p$  is the center frequency of the probe field,  $c$  is the speed of light in free space,  $n_{\text{eff}} = ck_p / \omega_p$  is the effective refraction index,  $\hat{\mathbf{e}}_p$  is the unit vector of the probe field polarization direction, and

$$\langle \psi(z) \rangle \equiv \frac{\int_{-\infty}^{+\infty} \zeta^*(z) \psi(z) dz}{\int_{-\infty}^{+\infty} |\psi(z)|^2 dz}. \quad (24)$$

### III. SURFACE POLARITON EXCITATION AND LINEAR PROPAGATION REGIME

Excitation and propagation of the SPs in this coupler free waveguide is described by the perturbative solution of the MB equations. The zeroth order of this perturbative method (i.e., the base state of the atomic medium) is obtained by assuming  $\Omega_p = 0$  and  $\partial/\partial t = 0$  in the Bloch equations. We thus obtain

$$\begin{aligned} \tilde{\rho}_{11}^{(0)} &= \frac{X_{23} \gamma_{31} (\Gamma_{44} - iX_{14})}{D}, \\ \tilde{\rho}_{22}^{(0)} &= \frac{X_{14} [\gamma_{42} \Gamma_{33} + \gamma_{32} \gamma_{43} - iX_{23} (\gamma_{42} + \gamma_{43})]}{D}, \end{aligned}$$

$$\begin{aligned}\tilde{\rho}_{33}^{(0)} &= \frac{iX_{14}X_{23}(\gamma_{42} + \gamma_{43})}{D}, & \tilde{\rho}_{44}^{(0)} &= \frac{iX_{14}X_{23}\gamma_{31}}{D}, \\ \tilde{\rho}_{14}^{(0)} &= \frac{-X_{23}X_{14}\Gamma_{44}\gamma_{31}}{D}, & \tilde{\rho}_{23}^{(0)} &= \frac{X_{14}X_{23}(\gamma_{42}\Gamma_{33} + \gamma_{32}\gamma_{43})}{D},\end{aligned}\quad (25)$$

where

$$\begin{aligned}X_1 &= \frac{\Omega_s}{d_{41}}, & X_2 &= \frac{\Omega_c}{d_{23}}, \\ X_{14} &= \frac{1}{d_{14}} - \frac{1}{d_{14}^*}, & X_{23} &= \frac{1}{d_{23}} - \frac{1}{d_{23}^*}, \\ D &= X_{23}\gamma_{31}\Gamma_{44} + X_{14}(\gamma_{42}\Gamma_{33} + \gamma_{32}\gamma_{43}) \\ &\quad - 2iX_{23}(\gamma_{31} + \gamma_{42} + \gamma_{43}).\end{aligned}\quad (26)$$

Here

$$\Gamma_{44} = \sum_{l<4} \gamma_{4l}, \quad \Gamma_{33} = \sum_{l<3} \gamma_{3l} \quad (27)$$

are the decay rates of the  $|4\rangle$  and  $|3\rangle$  atomic transitions, respectively, and  $\gamma_{jl} = (\Gamma_j + \Gamma_l)/2$  (with  $\Gamma_{j(l)}$  being the spontaneous emission from  $|j\rangle$  to  $|l\rangle$ ). Here the effect of collisional and dephasing rates and Doppler shifts are neglected by cooling the atomic sample to very low temperature (i.e., for suppression

of collisional effect one takes  $\gamma_{jl}^{\text{col}} \ll \Gamma_{j(l)}$  and for neglecting Doppler effect we assumed

$$W_D = \sqrt{\frac{k_B T}{M_e}} \ll \Gamma_{31}, \quad (28)$$

where  $T$  is the temperature of the atomic cell and  $M$  is the atomic mass of the rubidium) [43].

In the linear excitation of the system (i.e., first-order perturbation), the probe laser is switched on and the system possesses the time-dependent variations. However, this laser field is considered to be weak enough such that one can assume that the populations of the atomic states and the coherence between  $|1\rangle \rightarrow |4\rangle$  and  $|2\rangle \rightarrow |3\rangle$  transitions do not change significantly. In this order, the MB equations are linearized by assuming

$$\Omega_p(\mathbf{r}) = \epsilon \Omega_p^{(1)}(\mathbf{r}) \quad (29)$$

for  $\epsilon$  a weak perturbation parameter that represents small depletion of the  $|1\rangle$  atomic state and  $\tilde{\rho}_{ij} = \tilde{\rho}_{ij}^{(0)} + \epsilon \tilde{\rho}_{ij}^{(1)}$ . As a result one has

$$\begin{aligned}\tilde{\rho}_{21}^{(1)} &= a_{21}^{(1)} \zeta(z) F e^{i\phi}, & \tilde{\rho}_{31}^{(1)} &= a_{31}^{(1)} \zeta(z) F e^{i\phi}, \\ \tilde{\rho}_{42}^{(1)} &= a_{42}^{(1)} \zeta(z) F e^{i\phi}, & \tilde{\rho}_{43}^{(1)} &= a_{43}^{(1)} \zeta(z) F e^{i\phi},\end{aligned}\quad (30)$$

with  $\Omega_p^{(1)} = F e^{i\phi}$  and other  $\tilde{\rho}_{jl}^{(1)} = 0$ . Here  $\phi = K(\omega) - \omega t$  (with  $\omega$  being the frequency perturbation of the SPs) with

$$K(\omega) = \frac{\omega}{n_{\text{eff}} c} + \kappa_{13} \left\langle \zeta(z) \frac{X_{32}^{(1)} \tilde{\rho}_{32}^{(0)} - \zeta(z) \Omega_c (1 + D_{\text{cs}}) (\tilde{\rho}_{11}^{(0)} - \tilde{\rho}_{33}^{(0)}) + \zeta(z) \Omega_s (d_{42} - d_{13}) (D_s + |\zeta(z) \Omega_c|^2) \tilde{\rho}_{41}^{(0)}}{(d_{13} - d_{42}) \{D_{\text{cs}} + (d_{42} - d_{13}) [D_c (d_{12} + \omega) - |\zeta(z) \Omega_s|^2 (d_{43} + \omega)]\}} \right\rangle, \quad (31)$$

where

$$\begin{aligned}D_s &= (d_{12} + \omega)(d_{43} + \omega) - |\Omega_s|^2, \\ D_c &= |\Omega_c|^2 + (d_{42} + \omega)(d_{43} + \omega), \\ D_{\text{cs}} &= (D_c - |\Omega_s|^2)(D_s + |\Omega_c|^2), \\ X_{32}^{(1)} &= D_c (d_{42} - d_{13}) (D_s + |\Omega_c|^2) - (d_{42} + \omega)(1 + D_{\text{cs}}).\end{aligned}\quad (32)$$

Moreover, the atomic susceptibility can also be calculated by using the steady-state approximation of the Bloch equation, which is also expanded to the different order of perturbations. i.e.,

$$\chi_p \approx \chi_{\text{pp}}^{(1)}(\omega) + |\Omega_p(\mathbf{r})|^2 \chi_{\text{pp}}^{(3)}(\omega). \quad (33)$$

The linear susceptibility is then given by

$$\chi_{\text{pp}}^{(1)}(\omega) = \frac{N_a |\mathbf{p}_{13}| a_{31}^{(1)}}{\epsilon_0 |\mathbf{E}_p|}. \quad (34)$$

(The explicit expressions of the first-order perturbative solutions are given in Appendix C.)

The presented model can be easily realized in the experiment. For the NIMM one can use the Drude model parameters as [44]  $\epsilon_t = \epsilon_t' = 1$ ,  $\mu_t = \mu_t' = 1$ ,  $\epsilon_\infty = 6.5$ ,  $\mu_\infty = 6.5$ ,  $\omega_e = 1.37 \times 10^{16}$  Hz,  $\omega_m \approx 2.28 \times 10^{15}$  Hz,  $\gamma_e = 2.73 \times 10^{13}$  s $^{-1}$ , and  $\gamma_m = 10^{-3} \gamma_e$ , which is operated in the optical region

[45,46]. Moreover, the cold  $^{87}\text{Rb}$  atomic cell parameters are assumed to be [47,48]

$$\begin{aligned}|1\rangle &= |5S_{1/2}, F=2\rangle, & |2\rangle &= |5S_{1/2}, F=3\rangle, \\ |3\rangle &= |5P_{1/2}, F=2\rangle, & |4\rangle &= |5P_{3/2}, F=3\rangle.\end{aligned}\quad (35)$$

Here  $\lambda_c \approx 795$  nm and  $\lambda_s \approx 780$  nm are the two overlapped external cavities couple and signal diode lasers and

$$\lambda_p \approx 794.95 \text{ nm} \quad (36)$$

satisfies the

$$\lambda_c \approx \lambda_p \approx \lambda_s \quad (37)$$

condition,  $\kappa_{31} \approx 2.4 \times 10^9$ ,  $|\mathbf{p}_{13}| = 2.54 \times 10^{-27}$  C cm,  $\omega_p = 2.37 \times 10^{15}$  Hz,  $N_a = 8.75 \times 10^{10}$  cm $^{-3}$ , and  $\Gamma_{31} = \Gamma_{32} \approx \Gamma_{42} = 18.85$  MHz. The absorption and the dielectric constant of this cold Rb atomic cell as a function of  $\omega$  is depicted in Figs. 2. Figure 2(a) shows that the adjustment of couple and signal laser intensities and frequencies results in the narrow EIT windows in the various frequency deviations:  $\omega_{\text{EIT}} \approx 11.57$  MHz [49] for  $\Delta_c = -1.89$  MHz and  $\omega_{\text{EIT}} \approx 2.6$  MHz for  $\Delta_c = 8.8$  MHz with asymmetric absorption profile.

As a result of this narrow EIT window the dispersion of the atomic medium can be especially modulated. In the center of this window ( $\omega = \omega_{\text{EIT}} \approx 10$  MHz),  $\text{Re}(\chi_{\text{pp}}^{(1)}) \ll 1$

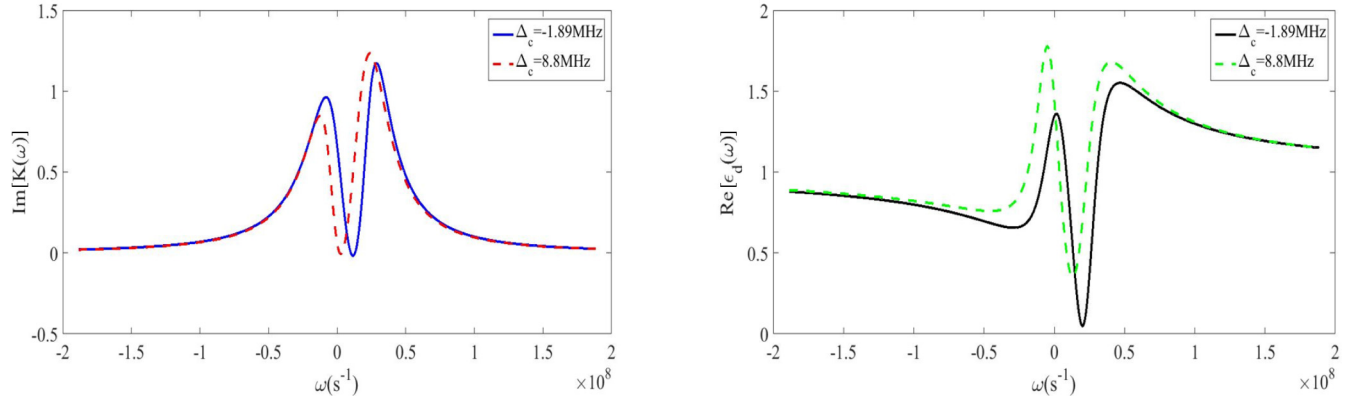


FIG. 2. Plot of (a) linear absorption and (b) the real part of the dielectric constant of atomic medium as a function of the frequency deviation ( $\omega$ ). The ultranarrow EIT window is observed due to the existence of the signal and couple laser fields and the resultant interference effects. Moreover, the optical properties of the atomic medium reach to the three level  $\Lambda$  type atomic system when the signal laser switched off  $\Omega_s = 0$ . The parameters used for these figures are  $\Omega_c = 34.56 \text{ MHz}$ ,  $\Omega_s = 30.79 \text{ MHz}$ ,  $\Delta_s = 15.71 \text{ MHz}$ , and  $\Delta_p = 11.31 \text{ MHz}$ .

and  $\text{Im}[K(\omega)]|_{\omega=\omega_{\text{EIT}}} \ll 1$  are satisfied simultaneously and therefore one can assume

$$\epsilon_d \approx 1 + \chi_{\text{pp}}^{(1)}. \quad (38)$$

These conditions provided that

$$\text{Im}[\epsilon_d(\omega)]|_{\omega=\omega_{\text{EIT}}} \ll 1 \quad (39)$$

and

$$\text{Re}[\epsilon_d(\omega)]|_{\omega=\omega_{\text{EIT}}} < 1 \quad (40)$$

are simultaneously observed in the atomic media.

These simulations demonstrate that  $\omega_{\text{EIT}}$  is suitable for SP propagation. The physical explanation of this frequency selection can be expressed as follows: the atomic medium and the NIMM layer have negligible absorption, the giant field concentration is achieved, and the atomic medium has also sufficient dispersion in this special EIT window which provides the lossless propagation of the SPs. The dispersion properties of the weak probe pulse can be achieved. The propagation properties of the SPs can be obtained by applying the expansion

of  $K(\omega)$  around the EIT frequency  $\omega_{\text{EIT}}$  in the form

$$K(\omega) = \sum_{m=0}^{\infty} \left( \frac{K_m}{m!} \right) (\omega - \omega_{\text{EIT}})^m, \quad (41)$$

where  $K_m = [\partial^m K(\omega)/\partial \omega^m]|_{\omega=\omega_{\text{EIT}}}$ . This equation shows that the propagation properties of the SP's wave (such as the group velocity and the GVD) in the center of the EIT window can be described by the various coefficients of the expansion.

To deeply look into the phenomena, the field factor and the reflection of this planar waveguide is represented in Fig. 3. Here the transmission coefficient of this three-layer waveguide is calculated similar to Eq. (17) as

$$t_{\text{td}} = \frac{t_{\text{tn}} t_{\text{nd}} e^{ik_{\text{nx}} l}}{1 + r_{\text{tn}} r_{\text{nd}} e^{2ik_{\text{nx}} l}}, \quad (42)$$

where  $t_{jl} = 1 + r_{jl}$  is the two layer transmission coefficient and

$$T = |t_{\text{td}}|^2, \quad R = |r_{\text{td}}|^2 \quad (43)$$

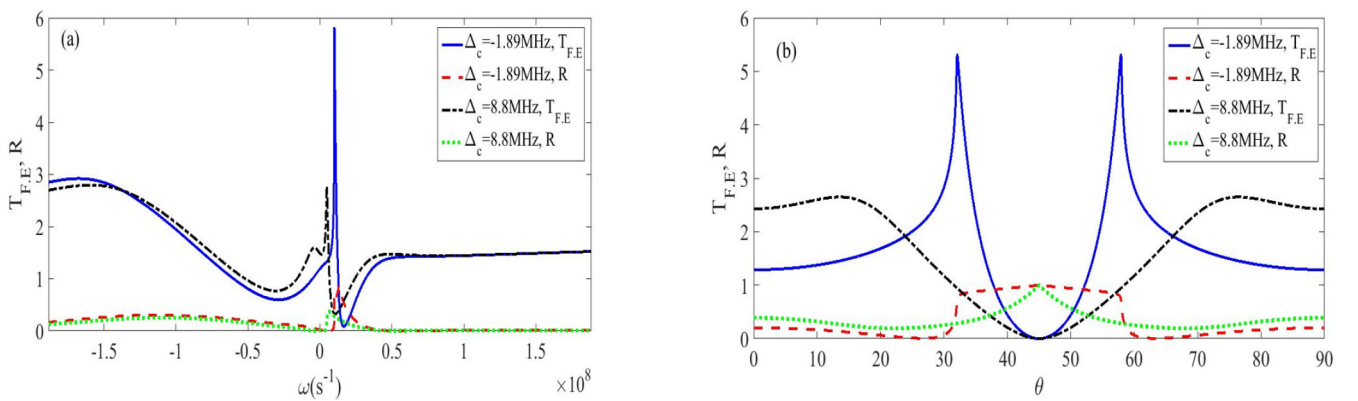


FIG. 3. Enhancement factor and the reflection coefficient is plotted as a function of (a) frequency deviation ( $\omega$ ) and (b) angle of incident ( $\theta$ ). In the ultranarrow EIT windows, giant field factor is observed with negligible reflection. The giant field factor (up to  $|E_{\text{nd}}|/E_0|^2$ ) in the EIT position promises the efficient excitation of SP modes in the coupler free scheme (see the text for details).

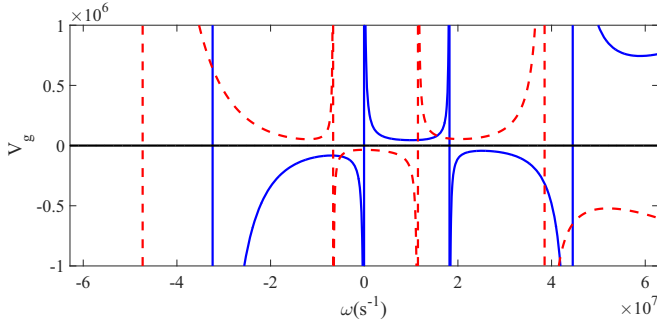


FIG. 4. Group velocity of the excited SP modes as a function of  $\omega$ . The group velocity can be switched from subluminal to superluminal with reduced atomic absorption. The blue solid line represents the SP group velocity for negative small coupling detunings, while the red dashed line denotes the behavior of  $\tilde{V}_g$  for positive  $\Delta_c$  and negligible absorption (see the text for details).

is the total transmission and reflection, respectively. Moreover, for the TE mode

$$T_{FE} = \left| \frac{E_{nd}}{E_{in}} \right|^2 = \left| \frac{\epsilon_t}{\epsilon_d} t_{nd} \right|^2, \quad (44)$$

where

$$|\mathbf{E}_{jl}|^2 = E_{x,jl}^2 + E_{y,jl}^2 + E_{z,jl}^2 \quad (45)$$

is assumed as a field factor of the waveguide. Here the transmission, reflection, and the linear optical properties of the atomic sample can be especially modulated and as a result one obtains  $T_{FE} \approx 5.73$  and  $R \approx 0.21$ . The other parameters for this efficient field enhancement are assumed as  $\theta \approx 63^\circ$ ,  $l = 95$  nm,  $\Delta_c = -1.89$  MHz, and  $\omega_{EIT} \approx 10$  MHz. Presented simulations also indicate that the probe field incident angle ( $\theta$ ) is a crucial parameter for obtaining giant field factor and reduced reflection as denoted from [Fig. 3(b)]. Therefore, giant field factor and reduced reflection, as well as the modulated optical absorption and dispersion of the atomic sample, can be simultaneously observed in this waveguide by setting the proper intensity, detuning of the driven laser fields, and suitable angle of incidence of the probe field which results in coherent excitation of the SP modes.

By investigation of the dispersion curves near resonance condition, one can observe that the normal and anomalous dispersion can be achieved by proper adjustment of the coupling field detuning. In order to further investigate, the group velocity of the SPs for various detunings of the coupled laser is depicted in Fig. 4. Existence of the signal field can lead to the sharp dispersion variation of the probe field in the EIT window. Therefore, one observes that the group velocity can be switched from subluminal to superluminal with reduced atomic absorption. The simulation also indicates that in the negative coupling field detuning the stable slow SPs can propagate in the EIT window ( $\tilde{V}_g \approx 1.50 \times 10^{-4}c$  for  $\omega_{EIT}$ ), while, for  $\Delta_c = 8.8$  MHz, the superluminal fast SPs ( $\tilde{V}_g \approx -7.97 \times 10^{-4}c$ ) propagate with negligible linear absorption. The modification of the SPs linear optical properties may lead to the formation of the shape preserved surface polaritonic solitons, rogue waves, and breathers with fairly long propagation length and controllable SP group velocity.

#### IV. EXCITATIONS AND PROPAGATION OF THE NONLINEAR SURFACE POLARITONS: SOLITON AND BREATHER SOLUTION

The rest of the results is arranged as follows: in Sec. IV A the NLSE is derived and the different (1 + 1)D temporal surface polaritonic solitons are observed. We investigated the possibility of the polaritonic rogue wave and breather formations in Sec. IV B.

##### A. Propagation of the bright and dark surface polaritonic solitons

The formation and propagation of the nonlinear SPs is investigated by applying the asymptotic expansions to the probe field Rabi frequency and the density matrix elements

$$\begin{aligned} \Omega_p(\mathbf{r}, t) &= \sum_1 \epsilon^l \Omega_p^{(l)}(\mathbf{r}, t), \\ \tilde{\rho}_{ij}(\mathbf{r}, t) - \tilde{\rho}_{ij}^{(0)} &= \sum_1 \epsilon^l \tilde{\rho}_{ij}^{(l)}(\mathbf{r}, t), \end{aligned} \quad (46)$$

where the different order of these expansions are considered to be a function of multiscale variables  $x^l = \epsilon^l x$  ( $l = 0, 1, 2$ ) and  $t_1 = \epsilon^l t$  ( $l = 0, 1$ ). Therefore, the position is scaled as a slow two step and time is set as a slower one scaled variable. By substituting into MB equations, the linear but inhomogeneous set of equations are achieved which can be solved order by order. In the second order, the density matrix elements are assumed as

$$\begin{aligned} \tilde{\rho}_{41}^{(2)} &= a_{41}^{(2)} \zeta(z) |F|^2 e^{-\alpha x_2}, & \tilde{\rho}_{41}^{(2)} &= a_{41}^{(2)} \zeta(z) |F|^2 e^{-\alpha x_2}, \\ \tilde{\rho}_{jj}^{(2)} &= a_{jj}^{(2)} \zeta(z) |F|^2 e^{-\alpha x_2}, & \tilde{\rho}_{11}^{(2)} &= -(\tilde{\rho}_{22}^{(2)} + \tilde{\rho}_{33}^{(2)} + \tilde{\rho}_{44}^{(2)}), \\ \tilde{\rho}_{j'1}^{(2)} &= a_{j'1}^{(2)} \zeta(z) \frac{\partial F}{\partial t_1} e^{i\theta}, & \tilde{\rho}_{4j'}^{(2)} &= a_{4j'}^{(2)} \zeta(z) \frac{\partial F}{\partial t_1} e^{i\theta}, \end{aligned}$$

with  $j = 2, 3, 4$  and  $j' = 2, 3$ . Moreover, the divergence free solution in this order can be obtained by taking  $\Omega_p^{(2)}(\mathbf{r}) = 0$  and

$$i \left( \frac{\partial F}{\partial x_1} + \frac{1}{V_g} \frac{\partial F}{\partial t_1} \right) = 0, \quad (47)$$

where  $V_g = 1/[\partial K(\omega)/\partial \omega]|_{\omega=\omega_{EIT}}$  is the group velocity of the SPs (the explicit expressions of the second-order density matrix elements is represented in Appendix D). In the third order ( $l = 3$ ), the solvability condition of the MB equations for  $\Omega_p^{(3)}$  requires

$$i \frac{\partial F}{\partial x_2} - \frac{K_2}{2} \frac{\partial^2 F}{\partial t_1^2} + W |F|^2 F e^{-2\alpha x_2} = 0, \quad (48)$$

where  $\alpha = \epsilon^2 \text{Im}[K(\omega)]$  represents the loss coefficient,  $K_2 = [\partial^2 K(\omega)/\partial \omega^2]|_{\omega=\omega_{EIT}}$  characterized the GVD of the medium, and  $W = [\hbar^2 \omega_p / (2c |\mathbf{p}_{13}|^2)] \chi_{pp}^{(3)}(z, \omega)$  is the self-phase

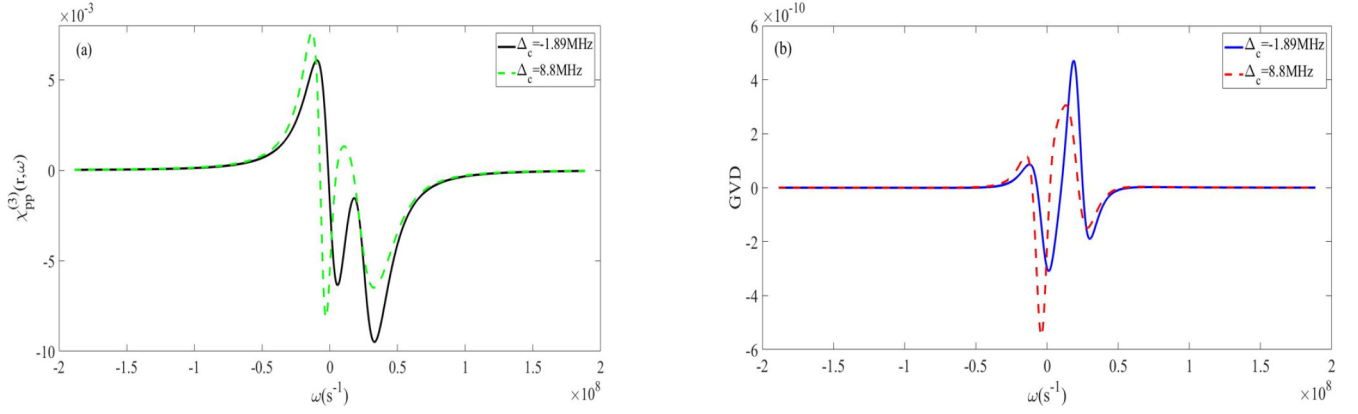


FIG. 5. Giant Kerr nonlinearity and sufficiently enhanced group-velocity dispersion. The Kerr nonlinearity ( $\text{Re}[\chi_{\text{pp}}^{(3)}(\mathbf{r}, \omega)]$ ) in panel (a) represents a giant self-focusing and self-defocusing optical Kerr in the EIT position. Panel (b) denotes the various types of ( $\Delta_c$ ) assisted normal and anomalous GVD as a function of frequency deviation. Balanced GVD-optical Kerr nonlinearity couples are achieved for both self-focusing and self-defocusing regimes. The parameters are the same as Fig. 2.

modulation coefficient of the cold atomic sample with

$$W = \left\langle \zeta(z) |\zeta(z)|^2 \frac{X_{32}^{(1)} a_{32}^{(2)} - \zeta(z) \Omega_c (1 + D_{\text{cs}}) (a_{11}^{(2)} - a_{33}^{(2)}) + \zeta(z) \Omega_s (d_{42} - d_{13}) (D_s + |\zeta(z) \Omega_c|^2) a_{41}^{(2)}}{(d_{13} - d_{42}) \{D_{\text{cs}} + (d_{42} - d_{13}) [D_c (d_{12} + \omega) - |\zeta(z) \Omega_s|^2 (d_{43} + \omega)]\}} \right\rangle. \quad (49)$$

Equation (48) is a partial differential equation (PDE) that can be obtained by applying the multiple fast-slow scales variable to the MB equations. The multiple scale method and the asymptotic expansions applied for the derivation of Eq. (48) are consistent with the general formalism of the PDEs developed in Refs. [50,51]. This equation has three main aspects. (i) The combination of the derivative with respect to  $x_2$ , second-order derivative with respect to  $t_1$  of the  $F$ , and existence of the nonlinear term  $|F|^2 F$  denotes that this equation is valid up to the third order of perturbation ( $l = 3$ ). (ii) This equation consists of a different order of perturbation which originates from the treatment of the fast two step scaled position and slow one step scaled time expansions. Therefore, derivative with respect to  $x_2$  and second-order derivative with respect to  $t_1$  become the same order of perturbation and can be observed in Eq. (48). (iii) The considered one step slow time variable admits that the derivative with respect to  $t_1$  should be considered in each order of perturbation [the details of the derivation of Eq. (48) are given in Appendix B].

The plot of Kerr nonlinearity (i.e.,  $\text{Re}[\chi_{\text{pp}}^{(3)}(\mathbf{r}, \omega)]$ ) and the GVD as a function of  $\omega$  is shown in Fig. 5. Panel (a) of this figure denotes that the optical Kerr nonlinearity can be significantly enhanced in the EIT window due to the existence of the mode confinement and modulation of the coupling field detuning. Moreover, by changing the sign of the Kerr nonlinearity, one observes that the coherently driven atomic sample has potential to act as a self-focusing and self-defocusing medium (i.e.,  $\chi_{\text{pp}}^{(3)}(\omega) > 0$  and  $[\chi_{\text{pp}}^{(3)}(\omega) < 0]$ ) by suitable field concentration in the atomic medium–NIMM interface, proper adjustment of the intensities, and detunings of driven laser fields. Furthermore, it is obvious from panel (b) that the GVD of the atomic medium in both focusing and defocusing regimes can be suitably modulated and as a result one can obtain the normal and anomalous GVD of the

SPs. Therefore, the various balanced GVD-Kerr nonlinearity couples can be achieved in this cold atomic medium in order for the propagation of the stable nonlinear SPs as bright and dark surface polaritonic solitons.

These results can be observed in an experiment by choosing the realistic parameters for the proposed waveguide:  $\Omega_s \approx 31$  MHz,  $\Omega_c \approx 35$  MHz,  $\Delta_s = 15.7$  MHz,  $\Delta_p \approx 11$  MHz, and  $\omega_{\text{EIT}} = 10^7$  s $^{-1}$ .

(i) For  $\Delta_c = -2$  MHz one has  $K_0 \approx (-2 + 0.016i)$  cm $^{-1}$ ,  $K_2 \approx (-4.42 + 0.21i) \times 10^{-12}$  cm $^{-1}$  s $^2$ ,  $\chi_{\text{pp}}^{(3)}(\omega, z = 0) = (4.7 + 0.9i) \times 10^{-3}$  cm $^2$  V $^{-2}$ , the field concentration

$$|E_{\text{nd}}|^2 \approx 5.8 |E_0|^2, \quad (50)$$

and  $n_2 = 3 \text{Re}[\chi_{\text{pp}}^{(3)}(z = 0, \omega_{\text{EIT}})] / \{2[1 + 2cK(\omega_{\text{EIT}})/\omega_p]\}^{1/2} \approx 7 \times 10^{-3}$  cm $^2$  V $^{-2}$ .

(ii) For  $\Delta_c \approx 9$  MHz we obtain

$$K_0 \approx (-1.3 + 0.054i)$$
 cm $^{-1}$ ,  $(51)$

$K_2 \approx (2.82 + 0.1i) \times 10^{-11}$  cm $^{-1}$  s $^2$ ,  $\chi_{\text{pp}}^{(3)}(\omega, z = 0) = (-1.3 + 0.24i) \times 10^{-3}$  cm $^2$  V $^{-2}$ ,  $|E_{\text{nd}}|^2 \approx 3|E_0|^2$ , and  $n_2 \approx -2 \times 10^{-3}$  cm $^2$  V $^{-2}$ .

Note that, in the present work, we have neglected the GVD related to the NIMM, which can be explained as follows: one can calculate the GVD related to the metamaterial layer by  $k_{2,n} = [\partial^2 k_n / \partial \omega_1^2]_{\omega_1 = \omega_p}$ . For the NIMM assumed in Sec. III one has  $k_{2,n} = (1.23 - 156i) \times 10^{-23}$  cm $^{-1}$  s $^2$ , which is  $10^{10}$  smaller than that of the GVD related to the atomic medium and therefore can be effectively neglected.

It can be realized that the imaginary parts of these quantities are much smaller compared to their real parts and, as a result, Eq. (48) can be written as

$$i \left( \frac{\partial}{\partial s} + \alpha \right) u + \frac{d_{\text{dis}}}{2} \frac{\partial^2 u}{\partial \sigma^2} + |u|^2 u = 0. \quad (52)$$

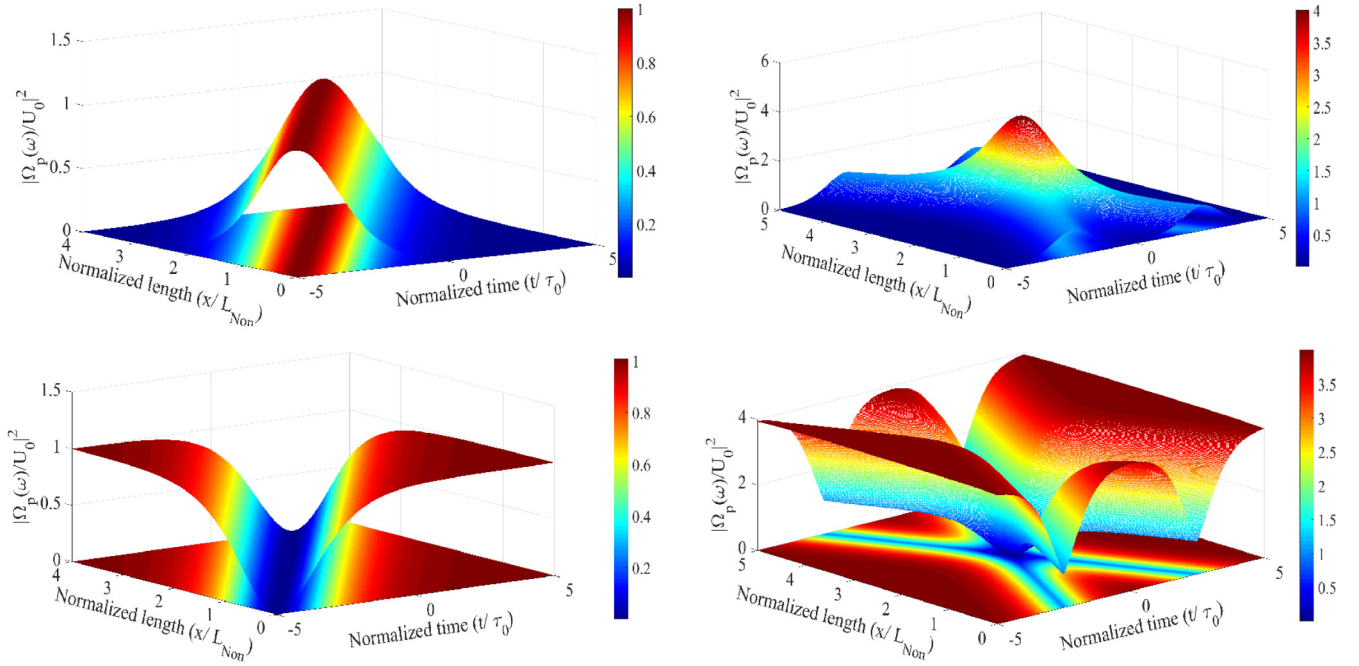


FIG. 6. Formation of bright and dark surface polaritonic solitons: the spatiotemporal dynamics of bright nonlinear SP's in the EIT window is depicted in (a) which demonstrates the existence of the bright mode surface polaritonic soliton. The stability of the two mode subluminal bright surface polaritonic solitons is investigated in (b) by plotting the collision of the corresponding SP solitons. The propagation of superluminal dark nonlinear SP's with negligible linear absorption is depicted in (c). Sufficient stability of these dark SP's [panel (d)] represents the fairly long distance propagation of the superluminal dark SP soliton.

where  $u = U/U_0$ ;  $U = \epsilon F e^{-\alpha x}$ ,  $U_0 = (\tilde{K}_2/\tilde{W})^{1/2}/\tau_0$  is the half-Rabi frequency of the probe field,  $s = x/L_{\text{non}}$  [with  $L_{\text{non}} = 1/(U_0^2|\tilde{W}|)$  being the nonlinear length of the medium], and  $d_{\text{dis}} = L_{\text{non}}/L_{\text{dis}}$ ;  $L_{\text{dis}} = \tau_0^2/\tilde{K}_2$  is the dispersion length and  $\tilde{K}_2$  and  $\tilde{W}$  are the real part of  $K_2$  and  $W(\omega = \omega_{\text{EIT}})$ , respectively. In the EIT position,  $\alpha \approx 0$  and, by taking  $\Delta_c = -2$  MHz,  $\tau_0 = 1 \mu\text{s}$ , and  $\Omega_p \approx 4$  MHz, one can assume the single soliton solution of the dark and bright surface polaritonic modes as

$$\Omega_{\text{pp}}^{(B)}(\mathbf{r}, t) = \sqrt{\frac{\tilde{K}_2}{(\tau_0^2 \tilde{W})}} \text{sech}[(t - x/\tilde{V}_g)/\tau_0] \times \exp[i(\tilde{K}_0 + 1/(2L_D))x], \quad (53)$$

$$\Omega_{\text{pp}}^{(D)}(\mathbf{r}, t) = \sqrt{\frac{\tilde{K}_2}{(\tau_0^2 \tilde{W})}} \tanh[(t - x/\tilde{V}_g)/\tau_0] \times \exp[i(\tilde{K}_0 + 1/(2L_D))x]. \quad (54)$$

Here  $\tilde{K}_0 = \text{Re}[K(\omega)]|_{\omega=\omega_{\text{EIT}}}$ . This set of solutions describes the bright and dark traveling waves with the group velocities  $\tilde{V}_g = \text{Re}[(1/[\partial K(\omega)/\partial \omega])|_{\omega=\omega_{\text{EIT}}}]$ . The corresponding electric fields of bright and dark waves are readily obtained as

$$\mathbf{E}_{\text{pp}}^{(B)}(\mathbf{r}, t) = \frac{\hbar}{|\mathbf{p}_{20}| \tau_0} \sqrt{\frac{\tilde{K}_2}{\tilde{W}}} \mathbf{u}_p(z) \text{sech} \left[ \tau_0^{-1} \left( t - \frac{x}{\tilde{V}_g} \right) \right] \times \exp i [K(\omega) + k(\omega_p) + 1/(2L_D) - (\omega + \omega_p)t] + \text{c.c.}, \quad (55)$$

$$\mathbf{E}_{\text{pp}}^{(D)}(\mathbf{r}, t) = \frac{\hbar}{|\mathbf{p}_{20}| \tau_0} \sqrt{\frac{\tilde{K}_2}{\tilde{W}}} \mathbf{u}_p(z) \tanh \left[ \tau_0^{-1} \left( t - \frac{x}{\tilde{V}_g} \right) \right] \times \exp i [K(\omega) + k(\omega_p) + 1/(2L_D) - (\omega + \omega_p)t] + \text{c.c.} \quad (56)$$

(i) For stable bright nonlinear SPs we have  $\tilde{W} \approx (2.88 + 0.56i) \times 10^{-11} \text{ cm}^{-1} \text{ s}^2$ ,  $L_{\text{non}} \approx 22 \text{ cm}$ ,  $L_{\text{dis}} = 23 \text{ cm}$ , and  $d_{\text{dis}} \approx 1$ . (ii) In order to observe the shape preserved dark nonlinear SPs one has  $\tilde{W} \approx (-7.96 + 3.30i) \times 10^{-12} \text{ cm}^{-1} \text{ s}^2$ ,  $\Omega_p \approx 5.95$  MHz,  $L_{\text{non}} \approx 0.35 \text{ cm}$ ,  $L_{\text{dis}} \approx 0.35 \text{ cm}$ , and  $d_{\text{dis}} = 1$ . The propagation of nonlinear bright and dark SPs is depicted in Fig. 6.

Evidently, the balanced dispersion with sufficient self-focusing coefficient is obtained by assuming  $\Delta_c = -2$  MHz,  $\Omega_p = 4$  MHz, and  $\theta \approx 63^\circ$ , results in the shape preserved robust nonlinear bright SP propagation with  $\tilde{V}_g \approx 1.49 \times 10^{-4} c$  slow group velocity, and as a result the bright surface polaritonic solitons can be excited and travel without significant distortion for a fairly long distance. Moreover, the peak power of the input probe laser pulse for the formation of the bright optical solitons can be calculated by Poynting's theorem [52]

$$P = \int_S dS (\mathbf{E}_{\text{pp}}^{(B)} \times \mathbf{H}_{\text{pp}}^{(B)}) \cdot \mathbf{e}_x, \quad (57)$$

where

$$\mathbf{H}_{\text{pp}}^{(B)} = \epsilon_0 c n_{\text{eff}} \mathbf{E}_{\text{pp}}^{(B)} \mathbf{e}_y \quad (58)$$

is the magnetic-field vector of the excited SPs. Therefore, one can obtain the bright input peak power as

$$\bar{P}_{\max}^{(B)} = 2\varepsilon_0 c n_{\text{eff}} S_0 |E_{\text{pp,max}}^{(B)}|^2 = 4.57 \mu\text{W}, \quad (59)$$

which is a very low input power to excitation of the surface polaritonic solitons.

Similarly, by relatively enhanced field concentration  $|E_{\text{nd}}|^2 \approx 3|E_0|^2$  as well as the negligible linear absorption and by taking into account  $\Delta_c \approx 9$  MHz,  $\theta = 60^\circ$ ,  $\Omega_s = 32$  MHz, and  $\Omega_p \approx 6$  MHz, the resonantly excited superluminal dark nonlinear SP (with  $\tilde{V}_g \approx -7.97 \times 10^{-4}c$ ) can be propagated without serious distortion. The physical explanation can be expressed as follows: the half probe field Rabi frequency is used for the excitation of the nonlinear SPs. In the bright SP solitons one has  $\text{Im}[K(\omega_{\text{EIT}})] = 0.0016 \text{ cm}^{-1}$  and  $\text{Im}[k(\omega_{\text{EIT}})] = 0.001 \text{ cm}^{-1}$ , which implies that  $\text{Im}[K(\omega_{\text{EIT}}) + k] \approx 0.003 \text{ cm}^{-1}$  and  $\Omega_{\text{pp}} \sim \Omega_{\text{pp}}^{(x=0)} e^{-\text{Im}[K(\omega_{\text{EIT}})+k]z} \approx 0.997 \Omega_{\text{pp}}^{(x=0)}$ . The small power attenuation as well as the balanced optical nonlinearity and dispersion effects result in the robust nonlinear bright SP propagation as a surface polaritonic soliton. Also, the propagation length of the excited SP's soliton along  $x$  direction can be estimated as  $L_{\text{Br}} = 3$  cm. Similarly, for the dark nonlinear SP propagation  $\text{Im}[K(\omega_{\text{EIT}})] \approx 0.02 \text{ cm}^{-1}$ , as a result  $\text{Im}[K(\omega_{\text{EIT}}) + k] \approx 0.022$  and  $|\Omega_{\text{pp}}|^2 \sim 0.67|\Omega_{\text{pp}}^{(x=0)}|^2$  after  $z = 10L_{\text{non}}$ . In this case, the highly self-defocusing nonlinearity and sufficient enhanced GVD in the resonant excitation are observed simultaneously, which demonstrates that the stable superluminal dark SP solitons without serious distortion in pulse envelope can propagate even up to 0.7 cm.

## B. Weak light surface polariton rogue waves and breathers solutions

### 1. First- and second-order surface polariton peregrine breathers

One of the outstanding features of the present work is the investigation of the SPRWB excitation and propagation in this coupler free planar waveguide. These nonlinear optical waves are the exact solutions of the standard self-focusing form of the nonlinear Schrodinger equation (NLSE)

$$i \frac{\partial u}{\partial s} + \frac{1}{2} \frac{\partial^2 u}{\partial \sigma^2} + |u|^2 u = 0. \quad (60)$$

This equation is obtained from Eq. (52) by neglecting the total loss of the optical waveguide. However, the suppression of the loss can be achieved by controlling the driven laser intensities and detunings. The loss reduction and modulated linear and nonlinear SPs can be achieved in the proposed waveguide by taking the experimentally feasible parameters to the NIMM and atomic medium as  $\Omega_s \approx 34.6$  MHz,  $\Omega_c = 30.8$  MHz,  $\Delta_s = 15.70$  MHz,  $\Delta_p = 1$  MHz, and  $\omega_{\text{EIT}} \approx 1$  MHz (center of the narrow EIT window) and, by taking  $\theta = 63.27^\circ$ , one has  $K_0 \approx (7.71 + 0.29i) \text{ cm}^{-1}$ ,  $K_1 = (1.01 + 0.36i) \times 10^{-6} \text{ cm}^{-1} \text{ s}$ ,  $\alpha = 0.001 \text{ cm}^{-1}$ ,  $K_2 = (-2.65 + 0.52i) \times 10^{-11} \text{ cm}^{-1} \text{ s}^2$ ,  $W = (3.48 - 0.05i) \times 10^{-11} \text{ cm}^{-1} \text{ s}^2$ ,  $\tau_0 = 8.5 \times 10^{-7} \text{ s}$ ,  $U_0 \approx 1$  MHz,  $L_{\text{non}} \approx 2.87$  cm,  $L_{\text{dis}} = 2.74$  cm, and  $L_{\text{abs}} = 1/\alpha \approx 620$  cm, and, as a result  $d_{\text{dis}} \approx 1.05$ , and Eq. (48) then was reduced to the standard NLSE with

sufficient probe laser field concentration  $|E_{\text{nd}}|^2 \approx 5.6|E_0|^2$  in the NIMM-atomic medium interface.

The standard NLSE admits a hierarchy of the localized rogue waves (breathers) solutions with a single maximum referred to as the peregrine rogue wave. This kind of breather can be written in terms of the polynomials  $G(s, \sigma)$ ,  $H(s, \sigma)$ , and  $D$  as [53]

$$u(s, \sigma) = \left[ 1 - \frac{G + iH}{D} \right] e^{is}. \quad (61)$$

The first-order solution is then given by

$$G = 4, \quad H = 4\sigma, \quad D = 1 + 4s^2 + 4\sigma^2. \quad (62)$$

After returning to original variables we have

$$\Omega_{\text{pp}}(x) = U_0 \left[ 1 - 4 \frac{(1 + 2ix/L_{\text{non}})}{1 + 4x^2/L_{\text{non}}^2 + 4[(t - x/\tilde{V}_g)/\tau_0]^2} \right] \times e^{i(\tilde{K}_\alpha + \frac{1}{L_{\text{non}}})x}. \quad (63)$$

These breathers are localized in time and space and the amplitude can be amplified by a factor of 3 in the  $(x, \tau) = (0, 0)$ . However, the mentioned breather can also be coherently generated and manipulated by the phase engineering techniques. The first-order solution is then rewritten in the form of  $\Omega_{\text{pp}}(x, t) = \psi_{\text{pp}}^{(1)}(x, t) e^{i\varphi_{\text{pp}}^{(1)}(x, t)}$  with

$$\psi_{\text{pp}}^{(1)}(x, t) = \sqrt{1 + \frac{8(4x^2/L_{\text{non}}^2 - 4(\tau/\tau_0)^2 - 1)}{(1 + 4x^2/L_{\text{non}}^2 - 4(\tau/\tau_0)^2)^2}}, \quad (64a)$$

$$\varphi_{\text{pp}}^{(1)}(x, t) = \left( \tilde{K}(\omega) + \frac{1}{L_{\text{non}}} \right) x - \frac{2x/L_{\text{non}}}{x^2/L_{\text{non}}^2 + (\tau/\tau_0)^2 - 3/4}, \quad (64b)$$

where  $\tau = x - t/\tilde{V}_g$ . Excitation and dynamics of the surface polaritonic rogue wave is represented in Fig. 7. The simulations indicate that the first-order SP peregrine wave can be generated in this polaritonic waveguide. We give two physical explanations for the formation and propagation of the SP peregrine rogue wave. First, the dynamics of the probe laser field under slowly varying amplitude approximation described by the standard NLSE admits the rogue wave solutions. Second, the NIMM-atomic medium interface can be effectively assumed as a nonlinear self-focusing system due to giant field concentration, suppressed atomic absorption, and controllable optical Kerr effect and, as a result, the proposed medium has potential for the propagation of the SP peregrine wave. The surface polaritonic plane wave then experiences dynamic growth as a result of MI in the proposed scheme. This SP amplification then results in the observation of the SP breather with intensity peaks up to  $|\Omega_{\text{pp,max}}|^2 \approx 9|U_0|^2$  [Fig. 7(a)] in a subluminal slow light level  $\tilde{V}_g \approx 3.35 \times 10^{-4}c$ . The generated SP peregrine breather can be propagated through the waveguide at the optimum probe field incidence  $\theta \approx 63.30^\circ$  with a very low generation peak power  $\bar{P}_{\max} \approx 4 \mu\text{W}$ .

The corresponding contour map of the excited SP peregrine breather [panel (b) of Fig. 7] also denotes that the amplitude of the excited wave is dramatically decreased out of the amplification region  $(x, \tau) \approx (0, 0)$ . However, the formations of this SP peregrine breather can be manipulated by phase

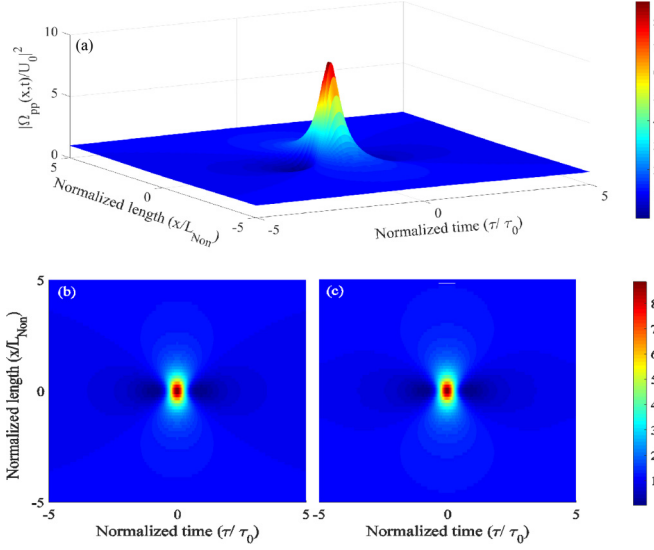


FIG. 7. Excitation of the weak light first-order surface polaritonic peregrine waves: 3D representation of the formation and evolution of the first-order surface polaritonic peregrine wave in the NIMM-quantum emitter interface is represented in panel (a). Panel (b) represents the contour map of panel (a), while the effect of phase engineering on the localization and the modulation of its contour map is represented in panel (c).

engineering of this rogue wave. Here the initial conditions can be taken as  $\psi_{pp}^{(1)} = \text{const}$  and  $\theta_{pp}^{(1)} = \theta_i$ ; however, for a weak probe laser the giant SP intensity is observed only for  $|\tau| \ll \tau_0$  and  $x \ll L_{\text{non}}$ . Therefore, the SP peregrine breather can also be observed by applying the small phase perturbation [Fig. 7(c)]. The above results can be verified by taking the numeric values to this waveguide,  $\tau \approx 0.7 \mu\text{s}$ ,  $x = 4.85 \text{ cm}$ , one has  $|\psi_{pp}^{(1)}| = 2.97$ ,  $\varphi_{pp}^{(1)} = 0.32$ , and  $\Omega_{pp}^{(1)} \sim U_0(1 - 0.3i)$ ; as a result the phase ( $\varphi$ ) can be applied as a perturbation parameter and in this case  $|\Omega_{pp,\text{max}}(\varphi_{pp})|^2 \approx 8.86|U_0|^2$  is also obtained.

The giant optical Kerr effect and the relatively large probe field factor in the NIMM-atomic medium interface results in the nonlinear focusing of the local polaritonic wave amplitude which leads to the generation of higher-order SP peregrine breathers in this planar waveguide. The polynomials for this second-order SP peregrine breather (super-rogue wave) is [54,55]

$$G = \left[ \left( \frac{x}{L_{\text{non}}} \right)^2 + \left( \frac{\tau}{\tau_0} \right)^2 + 3/4 \right] \\ \times \left[ \left( \frac{x}{L_{\text{non}}} \right)^2 + 5 \left( \frac{\tau}{\tau_0} \right)^2 + \frac{3}{4} \right], \\ H = \left( \frac{\tau}{\tau_0} \right) \left[ \left( \frac{\tau}{\tau_0} \right)^2 - 3 \left( \frac{x}{L_{\text{non}}} \right)^2 \right] \\ + \left( \frac{\tau}{\tau_0} \right) \left\{ 2 \left[ \left( \frac{x}{L_{\text{non}}} \right)^2 + \left( \frac{\tau}{\tau_0} \right)^2 \right]^2 - \frac{15}{8} \right\},$$

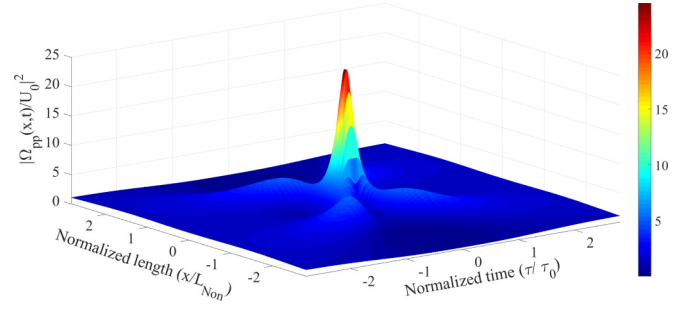


FIG. 8. Observation of the second-order surface polariton peregrine breathers. The giant SP amplitude enhancement  $|\Omega_{pp}^{(2)}| \approx 4.58U_0$  with sufficient localized distribution is achieved.

$$\mathcal{D} = \frac{1}{3} \left[ \left( \frac{x}{L_{\text{non}}} \right)^2 + \left( \frac{\tau}{\tau_0} \right)^2 \right]^3 \\ + \frac{1}{4} \left[ \left( \frac{x}{L_{\text{non}}} \right)^2 - 3 \left( \frac{\tau}{\tau_0} \right)^2 \right] \\ + 3 \left[ 12 \left( \frac{x}{L_{\text{non}}} \right)^2 + 44 \left( \frac{\tau}{\tau_0} \right)^2 + 1 \right]. \quad (65)$$

The dynamics of the second-order SP peregrine breather is represented in Fig. 8. This simulation indicates that the SP super-rogue wave has a maximum amplitude in  $(x, \tau) = (0, 0)$  up to  $|\Omega_{pp}^{(2)}|^2 \approx 25|U_0|^2$ . The obtained intensity peak crucially depends on the loss mechanism of the medium, i.e., absorption of the atomic medium and ohmic loss of the NIMM, field concentration in the NIMM-atomic medium interface, and enhancement of the optical self-focusing. Therefore, small peak attenuation is expected due to the weak losses of this polaritonic waveguide.

In order to see the SP super rogue wave, we choose the experimental parameter of the atomic ensembles and the NIMM layer. One has  $\Delta_c = 1.9 \text{ MHz}$ ,  $\Delta_p = 1 \text{ MHz}$ ,  $\Omega_c = 31 \text{ MHz}$ ,  $\Omega_s = 25 \text{ MHz}$  in the  $\omega_{\text{EIT}} \approx 0.7 \text{ MHz}$ ,  $\text{Im}(K_0) = 0.01 \text{ cm}^{-1}$ ,  $\text{Im}[k(\omega_{\text{EIT}})] = 0.007 \text{ cm}^{-1}$ ,  $\text{Im}[K(\omega_{\text{EIT}}) + k(\omega_{\text{EIT}})] \approx 0.02$  and, with subluminal group velocity  $\tilde{V}_g \approx 4500 \text{ m/s}$ , field attenuation  $|\Omega_{pp}(x = 3L_{\text{non}}, t = x/\tilde{V}_g)| \sim 0.84U_0$  can be achieved and hence SP surface rogue wave with  $|\Omega_{pp,\text{max}}^{(2)}| \approx 21|U_0|^2$  and very low generation power  $\bar{P}_{\text{max}} \approx 4 \mu\text{W}$  is observed in the  $\Delta x \approx 0.52 \text{ cm}$  and  $\Delta \tau = 0.03\tau_0$  intervals. The observation of the extreme SP super-rogue waves may have potential applications in many fields of plasmonics such as the optical resonators, nanoantennas and amplifiers, subwavelength imaging and photolithography, etc.

## 2. Observation of the periodic surface polariton breathers

The standard NLSE admits other exact solutions which are periodic in the  $\sigma$  and  $s$  directions. The special first-order solution pointed out by Akhmediev and Korneev can be assumed as

$$\Omega_{pp,AB}^{(1)}(s, \sigma) = U_0 \left[ 1 + \frac{2[1 - 2a] \cosh(bs) + ib \sinh(bs)}{\sqrt{2a} \cos(\Omega\sigma) - \cosh(bs)} \right] \\ \times e^{i(\tilde{K}_\alpha + \frac{1}{L_{\text{non}}})x}, \quad (66)$$

which, after returning to the original variable, we have

$$\Omega_{pp,AB}^{(1)}(x, \tau) = U_0 \left[ \frac{(1 - 4a) \cosh(bx/L_{non}) + \sqrt{2a} \cos(\Omega\tau/\tau_0) + ib \sinh(bx/L_{non})}{\sqrt{2a} \cos(\Omega\tau/\tau_0) - \cosh(b\sigma)} \right] e^{i(\bar{k}_\alpha + \frac{1}{L_{non}})x}, \quad (67)$$

where  $a$  is the modulation parameter, real variable  $b = \sqrt{8a(1-2a)}$ , and  $\Omega = 2\sqrt{1-2a}$  are the parametric gain coefficient and the modulation frequency, respectively. The evolution and propagation of the Akhmediev breathers is depicted in Fig. 9. Here, for  $0 < a < 0.5$ , the instability can be periodically modulated and as a result the plane wave ( $a = 0$ ) possesses a significant pulse shape and converts into a train of periodic waves along  $\tau$  axis with  $T = \pi/\sqrt{1-2a}$  period.

The physical explanation of this effect can be expressed as follows. The initial surface polaritons can be assumed as a plane wave which can experience an exponential growth due to gain coefficient and as a result the SP's amplitude amplified significantly by means of the growth factor  $b$  in a certain period of time. Existence of the modulated self-focusing nonlinearity of the atomic medium, negligible loss of the waveguide, and the giant electric-field concentration leads to the time domain modulation of the instability. Therefore, amplified SP's amplitude in time domain is observed and the first-order SP Akhmediev breathers can be excited and propagated in this waveguide.

Efficient propagation of the SP Akhmediev breather can also be observed in an experiment by taking  $v_1 \equiv \sqrt{2a} = 0.71$ ,  $\Omega \approx 1.41$ ,  $b = 1$ ,  $T = 1.39\pi$ ,  $\Delta\tau \approx 1.7\tau_0$ , and  $\Delta x = 0.1L_{non}$  and  $|\Omega_{pp,AB}| \approx 2.72U_0$  maximum peak of the SPs is obtained. By choosing  $a = 0.32$ ,  $T = 1.67\pi$  and  $|\Omega_{pp,AB}| \approx 2.41U_0$ . As

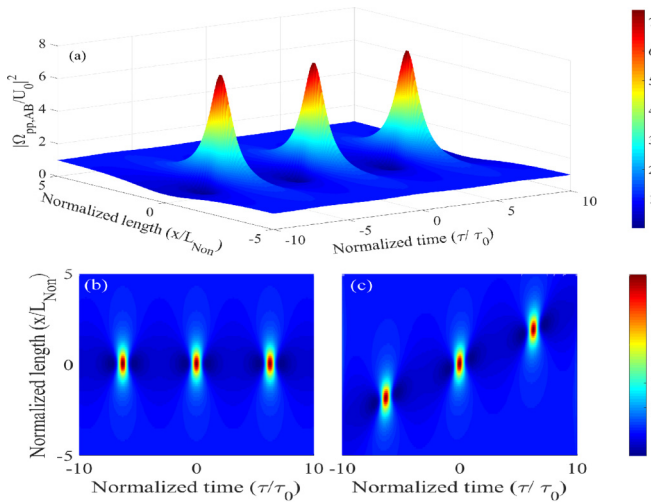


FIG. 9. Dynamics of the SP Akhmediev breathers. The dynamics of the probe field intensity  $|\Omega_{pp,AB}/U_0|^2$  as a function of normalized length  $x/L_{Non}$  and normalized time  $(t - z/\tilde{V}_g)/\tau_0$  is represented in panel (a). The parameters used are  $\Omega = 1.2$ ,  $a = 0.32$ , and  $b = 0.96$ . Panel (b) represents the corresponding contour map of the panel (a) when the modulation frequency is set as real values. This plot shows the zero velocity of the SP Akhmediev breather propagation. (c) The nonzero velocity of the SP Akhmediev breathers: this breather propagation can be achieved by considering the complex frequency modulation. The values are the same as panel (a) with  $\Omega_i = 0.3$ .

a result, by increasing the modulation parameter  $a$ , the strong localizations of the SPs in both dimensions can be achieved; however, the peak intensity of the rogue waves is decreased simultaneously. The proper set of the modulation parameter in order to obtain the maximum peak intensity is  $a = 0.25$ .

The nonzero velocity of the SP Akhmediev breathers can also be observed in the waveguide by inducing the imaginary parts to the modulation frequency (i.e.,  $\Omega = \Omega_r + i\Omega_i$ ). The exact solution in this case can be obtained by using the Darboux transformation

$$\Omega_{pp,AB} = U_0 \left[ \frac{\mathcal{G}_1 + i\mathcal{G}_2}{\mathcal{D}_G} \right] e^{is'}, \quad (68)$$

where

$$\begin{aligned} \mathcal{D}_G &= \cosh\left(\frac{\Omega_r lx}{L_{non}} + \vartheta_i\right) \cosh(2\xi_i) \\ &\quad - \cos\left(\frac{\Omega_i lx}{L_{non}} - \vartheta_r\right) \sin(2\xi_r), \\ \mathcal{G}_1 &= \cosh\left(\frac{\Omega_r lx}{L_{non}} + \vartheta_i\right) [\cosh(2\xi_i) - 2l \sin(2\xi_r)] \\ &\quad + \cos\left(\frac{\Omega_i lx}{L_{non}} - \vartheta_r\right) [2l \cosh(2\xi_i) - \sin(2\xi_r)], \\ \mathcal{G}_2 &= 2l \left[ \cos(2\xi_r) \sinh\left(\frac{\Omega_r lx}{L_{non}} + \vartheta_i\right) \right. \\ &\quad \left. - \sin\left(\frac{\Omega_i lx}{L_{non}} - \vartheta_r\right) \sinh(2\xi_i) \right]. \end{aligned} \quad (69)$$

In order to obtain the above equation, we used

$$\begin{aligned} \vartheta_{r(i)} &= \Omega_{r(i)} \left( t + \frac{v_1 x}{L_{non}} \right), \\ p &= \sqrt{\left(1 + \frac{\Omega_r}{2}\right)^2 + \left(\frac{\Omega_i}{2}\right)^2}, \\ q &= \sqrt{\left(1 + \frac{\Omega_r}{2}\right)^2 + \left(\frac{\Omega_i}{2}\right)^2}, \\ \cos(2\xi_r) &= \frac{\Omega_r}{(p+q)}, \quad \cosh(2\xi_i) = \frac{(p+q)}{2}. \end{aligned} \quad (70)$$

The result of these calculations is depicted in Fig. 9(c). It can be noticed that the train of the pulses travels with the nonzero velocity while the propagation direction of the breathers possesses small angles with respect to the  $\tau$  axis. The explanation of this effect can be expressed as follows. The complex eigenvalues (i.e.,  $e_1 = v_1 + il$ ) of the Darboux transformation results in the complex modulation frequency. The zero velocity propagation of the Akhmediev breather was obtained for pure imaginary of the eigenvalue, while the real value of the frequency modulation and consequently the

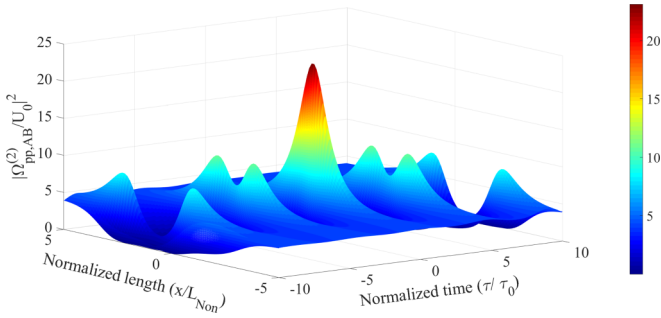


FIG. 10. Dynamics of the higher-order NLSE solution: the collision of the SP Akhmediev breathers is plotted as a function of normalized time ( $\tau/\tau_0$ ) and normalized length ( $z/L_{\text{Non}}$ ). The picture shows the significant time and space localizations of the SP breather. The parameters used are  $a_2 = 0.30$ ,  $\Omega_i = 0.3$ ,  $l_1 = 0.6$ , and  $l_2 = -0.6$ . Other parameters are the same as Fig. 9.

real value of the complex eigenvalue of this transformation is responsible for the nonzero propagation of the Akhmediev breathers.

The high SP breather intensity with sufficient localization can also be achieved in this coupler free polaritonic waveguide by investigation of the collision between the two independent Akhmediev breathers with different frequency modulations. In this case the higher-order NLSE can be solved as [56]

$$\Omega_{\text{pp,AB}}^{(2)} = \Omega_{\text{pp,AB}}^{(1)} + \frac{2(e_1^* - e_1')s_{12}m_{12}^*}{|s_{12}|^2 + |m_{12}|^2}. \quad (71)$$

$$\Omega_{\text{pp,KMB}}^{(1)}(x, \tau) = U_0 \left[ \frac{(1 - 4a) \cos(bx/L_{\text{non}}) + \sqrt{2a} \cosh(\Omega\tau/\tau_0) - ib \sin(bx/L_{\text{non}})}{\sqrt{2a} \cosh(\Omega\tau/\tau_0) - \cos(bx/L_{\text{non}})} \right] e^{i(\tilde{K}_a + \frac{1}{L_{\text{non}}})x}. \quad (73)$$

This SP breather is then periodic in the  $x$  axis and localized in the  $\tau$  domain. The dynamics of the SP Kuznetsov-Ma breathers is represented in Fig. 11. It can be realized that the breather is

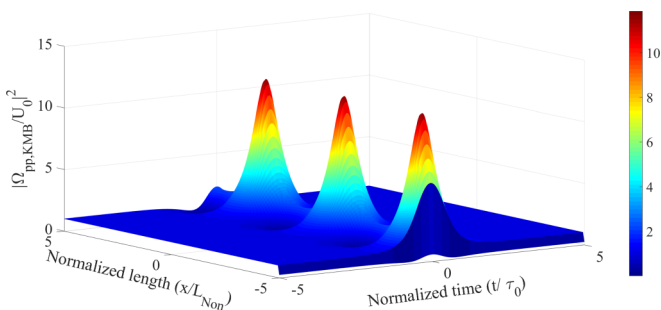


FIG. 11. Observation of the SP Kuznetsov-Ma breathers. This solution of the standard NLSE is localized in both in  $x$  and  $\tau$  axes and propagates along the interface of the NIMM-atomic medium interface. The probe field intensity  $|\Omega_{\text{p}}/U_0|^2$  has maximas along the propagation direction with giant SP intensity peaks. The propagation length can be greatly enhanced compared to that of the temporal soliton. The parameter used for this simulation is  $\Omega = 1.26$ ,  $b = 1.5$ , and  $T_z \approx 1.3\pi$ .

The exact coefficient of Eq. (71) can be found in Appendix E. This solution leads to the collision of the two SP Akhmediev breather as depicted in Fig. 10. Here the existence of two near zero velocity SP breather modes with the two identical frequency modulations  $\Omega(\Omega')$  and the two eigenvalues  $e_1 = \nu_1 + il$ ,  $e_1' = \nu_2 + il'$  results in the formation of the giant SP intensity peak in the  $(x, \tau) = (0, 0)$ . The maximum SP intensity peak can be estimated as  $|\Omega_{\text{pp,AB}}^{(2)}|^2 \approx 25U_0^2$ . However, the peak intensity of this breather is limited by the different loss mechanisms in the present waveguide. The above results can be checked by assuming the real parameters in this waveguide:  $\omega_{\text{EIT}} \approx 1$  MHz,  $\Omega_s = 30$  MHz and  $\Omega_c \approx 35$  MHz,  $\text{Im}[K(\omega_{\text{EIT}})] = 0.001 \text{ cm}^{-1}$  and  $\text{Im}[k(\omega_{\text{EIT}})] \approx 0.004 \text{ cm}^{-1}$ ,  $\tilde{K}_\alpha(\omega_{\text{EIT}}) = \text{Im}[K + k] \approx 0.005$ ,  $x_0 = 2.7 \text{ cm}$ ,  $|\Omega_{\text{pp}}| \approx 0.98U_0$  and the loss can be effectively suppressed and one has  $|\Omega_{\text{pp,AB}}^{(1)}(x = 0, \tau = 0)/U_0| = 2.38$ ; therefore, the highly localized intense SP mode can be observed in the presented waveguide as a result of two SP Akhmediev breather mode collisions. The corresponding intensity peak of this breather is estimated as

$$|\Omega_{\text{pp,AB}}^{(2)}(x = 0, \tau = 0)|^2 = 22.61|U_0|^2. \quad (72)$$

The first- and second-order SP Akhmediev breathers can be propagated only for  $0 < a < 0.5$  frequency modulation. The limiting case  $a \rightarrow 0.5$  corresponds to the first- and second-order SP peregrine rogue waves and the solution for  $a > 0.5$  referred to as Kuznetsov-Ma breathers, which are

modulated in the position domain with period

$$T_z = \frac{\pi}{\sqrt{2a(1-2a)}}. \quad (74)$$

Moreover, compared to that of the SP Akhmediev breathers,

$$b = \sqrt{8a(2a-1)}, \quad \Omega = 2\sqrt{2a-1} \quad (75)$$

are the instability growth rate and the modulation frequency of the SP Kuznetsov-Ma breathers.

The physical origin of the generation of the SP Kuznetsov-Ma breathers is the modulation instability in the position domain. Here the initial surface polaritonic plane wave is assumed to be excited in this waveguide which can be amplified through the propagation in the NIMM-atomic medium interface due to MI. Therefore, the train of intense SP pulse along with the mentioned interface can travel in this waveguide with sufficiently enhanced propagation length compared to that of the temporal solitons. This kind of SP breather can also be observed in an experiment by considering the above system parameter:  $x_0 = -2.7 \text{ cm}$ ,  $\tilde{K}_\alpha(\omega_{\text{EIT}}) = 0.004 \text{ cm}^{-1}$  by propagation after  $7L_{\text{non}}$  we have  $|\Omega_{\text{pp,KMB}}(x, t)| \sim 0.93|U_0|$  and  $\tilde{V}_g \approx 4460 \text{ m/s}$ , which represents the robust intense SP pulse compared to that of the temporal soliton. The existence

of this kind of SP pulse with enhanced propagation length may have potential applications in many fields of plasmonics.

## V. CONCLUSION

To sum up, the coherent excitation and propagation of the surface polaritonic solitons, rogue waves, and breathers are proposed using a coupler free waveguide which consists of three layers: transparent medium, NIMM layer, and cold four level  $N$  type atomic medium. In the linear excitation, the giant field concentration ( $|E_{\text{nd}}|^2 \approx 6|E_0|^2$ ) and modified dielectric constant of the atomic susceptibility are achieved in the obtained narrow EIT window.

Existence of giant controllable Kerr nonlinearity also results in the stable propagation of (1 + 1)D temporal bright and dark surface polaritonic solitons with controllable SP group velocity. Therefore, the linear and nonlinear optical properties of the SP's in this optical waveguide can be modified, which makes it possible to use this polaritonic device as a SPRWB propagator. The results for the surface polaritonic breathers and rogue waves have some interesting aspects.

(i) The first- and second-order peregrine rogue wave is observed in this coupler free polaritonic waveguide. The considerable intensity enhancement and the sufficient localization of the SPs are observed by the investigation of the various order of peregrine breather dynamics.

(ii) The different zero and nonzero velocities and collisions of the two modes near the zero velocity surface polaritonic Akhmediev breather is achieved in our proposed waveguide.

(iii) The train of the intensity enhanced SPs with effective time and space localizations is also observed in this coupler free optical waveguide due to the existence of the MI and as a result the giant propagation length of the SPs can be achieved.

The localized SPs with the giant intensity and enhanced propagation length due to rogue wave and breather formations may have potential applications in the fields of plasmonics and optical communication systems.

## ACKNOWLEDGMENTS

B.C.S. acknowledges NSERC funding from Canada and support from India's Science and Engineering Research Board (SERB) Visiting Advanced Joint Research Faculty (VAJRA) Scheme.

## APPENDIX A: EXACT SOLUTION OF THE BLOCH EQUATIONS

The dynamics of the density matrix elements of the proposed four level  $N$  type cold atomic medium can be expressed as follows:

$$i\left(\frac{\partial}{\partial t} + \Gamma_{21}\right)\tilde{\rho}_{22} - i\Gamma_{42}\tilde{\rho}_{44} - i\Gamma_{32}\tilde{\rho}_{33} + \frac{1}{2}[\zeta^*(z)\Omega_c^*\tilde{\rho}_{32} - \zeta(z)\Omega_c\tilde{\rho}_{23}] = 0, \quad (\text{A1a})$$

$$i\left(\frac{\partial}{\partial t} + \Gamma_{33}\right)\tilde{\rho}_{33} - i\Gamma_{43}\tilde{\rho}_{44} + \frac{1}{2}[\zeta(z)\Omega_c\tilde{\rho}_{23} - \zeta^*(z)\Omega_c^*\tilde{\rho}_{32} + \zeta(z)\Omega_p\tilde{\rho}_{13} - \zeta^*(z)\Omega_p\tilde{\rho}_{31}] = 0, \quad (\text{A1b})$$

$$i\left(\frac{\partial}{\partial t} + \Gamma_{44}\right)\tilde{\rho}_{44} + \frac{1}{2}[\zeta(z)\Omega_s\tilde{\rho}_{14} - \zeta^*(z)\Omega_s^*\tilde{\rho}_{41}] = 0, \quad (\text{A1c})$$

$$i\left(\frac{\partial}{\partial t} + d_{21}\right)\tilde{\rho}_{21} + \frac{1}{2}\zeta^*(z)\Omega_c^*\tilde{\rho}_{31} - \frac{1}{2}\zeta(z)\Omega_s\tilde{\rho}_{24} - \frac{1}{2}\zeta(z)\Omega_p\tilde{\rho}_{23} = 0, \quad (\text{A1d})$$

$$i\left(\frac{\partial}{\partial t} + d_{31}\right)\tilde{\rho}_{31} + \frac{1}{2}\zeta(z)\Omega_c\tilde{\rho}_{21} - \frac{1}{2}\zeta(z)\Omega_s\tilde{\rho}_{34} + \frac{1}{2}\zeta(z)\Omega_p(\tilde{\rho}_{11} - \tilde{\rho}_{33}) = 0, \quad (\text{A1e})$$

$$i\left(\frac{\partial}{\partial t} + d_{41}\right)\tilde{\rho}_{41} - \frac{1}{2}\zeta(z)\Omega_p\tilde{\rho}_{43} + \frac{1}{2}\zeta(z)\Omega_s(\tilde{\rho}_{11} - \tilde{\rho}_{44}) = 0, \quad (\text{A1f})$$

$$i\left(\frac{\partial}{\partial t} + d_{32}\right)\tilde{\rho}_{32} + \frac{1}{2}\zeta(z)\Omega_c(\tilde{\rho}_{22} - \tilde{\rho}_{33}) + \frac{1}{2}\zeta(z)\Omega_p\tilde{\rho}_{12} = 0, \quad (\text{A1g})$$

$$i\left(\frac{\partial}{\partial t} + d_{42}\right)\tilde{\rho}_{42} - \frac{1}{2}\zeta(z)\Omega_c\tilde{\rho}_{43} + \frac{1}{2}\zeta(z)\Omega_s\tilde{\rho}_{12} = 0, \quad (\text{A1h})$$

$$i\left(\frac{\partial}{\partial t} + d_{43}\right)\tilde{\rho}_{43} + \frac{1}{2}\zeta(z)\Omega_s\tilde{\rho}_{13} - \frac{1}{2}\zeta^*(z)\Omega_c^*\tilde{\rho}_{42} - \frac{1}{2}\zeta^*(z)\Omega_p^*\tilde{\rho}_{41} = 0, \quad (\text{A1i})$$

where  $d_{21} = (\Delta_p - \Delta_c) + i\gamma_{21}$ ,  $d_{31} = \Delta_p + i\gamma_{31}$ ,  $d_{41} = \Delta_s + i\gamma_{41}$ ,  $d_{32} = \Delta_c + i\gamma_{32}$ ,  $d_{42} = (\Delta_c + \Delta_s - \Delta_p) + i\gamma_{42}$ , and  $d_{43} = (\Delta_s - \Delta_p) + i\gamma_{43}$ . The definition of the atomic decay rates is given in Sec. III.

**APPENDIX B: DETAILS OF DERIVATION OF EQ. (48)**

In this Appendix, we give some steps of the nonlinear Schrödinger equation derivation; the asymptotic expansions of the Bloch equations for the  $l$ th order read

$$i\left(\frac{\partial}{\partial t_0} + \Gamma_{21}\right)\tilde{\rho}_{22}^{(l)} - i\Gamma_{42}\tilde{\rho}_{44}^{(l)} - i\Gamma_{32}\tilde{\rho}_{33}^{(l)} + \frac{1}{2}(\zeta^*(z)\Omega_c^*\tilde{\rho}_{32}^{(l)} - \zeta(z)\Omega_c\tilde{\rho}_{23}^{(l)}) = A^{(l)}, \quad (\text{B1})$$

$$i\left(\frac{\partial}{\partial t_0} + \Gamma_{33}\right)\tilde{\rho}_{33}^{(l)} - i\Gamma_{43}\tilde{\rho}_{44}^{(l)} + \frac{1}{2}(\zeta(z)\Omega_c\tilde{\rho}_{23}^{(l)} - \zeta^*(z)\Omega_c^*\tilde{\rho}_{32}^{(l)} + \zeta(z)\Omega_p^{(l)}\tilde{\rho}_{13}^{(0)} - \zeta^*(z)\Omega_p^{(l)}\tilde{\rho}_{31}^{(0)}) = B^{(l)}, \quad (\text{B2})$$

$$i\left(\frac{\partial}{\partial t_0} + \Gamma_{44}\right)\tilde{\rho}_{44}^{(l)} + \frac{1}{2}(\zeta(z)\Omega_c\tilde{\rho}_{14}^{(l)} - \zeta^*(z)\Omega_c^*\tilde{\rho}_{41}^{(l)}) = C^{(l)}, \quad (\text{B3})$$

$$i\left(\frac{\partial}{\partial t_0} + d_{21}\right)\tilde{\rho}_{21}^{(l)} + \frac{1}{2}\zeta^*(z)\Omega_c^*\tilde{\rho}_{31}^{(l)} - \frac{1}{2}\zeta(z)\Omega_s\tilde{\rho}_{24}^{(l)} - \frac{1}{2}\zeta(z)\Omega_p^{(l)}\tilde{\rho}_{23}^{(0)} = D^{(l)}, \quad (\text{B4})$$

$$i\left(\frac{\partial}{\partial t_0} + d_{31}\right)\tilde{\rho}_{31}^{(l)} + \frac{1}{2}\zeta(z)\Omega_c\tilde{\rho}_{21}^{(l)} - \frac{1}{2}\zeta(z)\Omega_s\tilde{\rho}_{34}^{(l)} - \frac{1}{2}\zeta(z)\Omega_p^{(l)}(\tilde{\rho}_{11}^{(0)} - \tilde{\rho}_{33}^{(0)}) = e^{(l)}, \quad (\text{B5})$$

$$i\left(\frac{\partial}{\partial t_0} + d_{41}\right)\tilde{\rho}_{41}^{(l)} + \frac{1}{2}\zeta(z)\Omega_s(\tilde{\rho}_{11}^{(l)} - \tilde{\rho}_{44}^{(l)}) - \frac{1}{2}\zeta(z)\Omega_p^{(l)}\tilde{\rho}_{43}^{(0)} = F^{(l)}, \quad (\text{B6})$$

$$i\left(\frac{\partial}{\partial t_0} + d_{32}\right)\tilde{\rho}_{32}^{(l)} + \frac{1}{2}\zeta(z)\Omega_c(\tilde{\rho}_{22}^{(l)} - \tilde{\rho}_{33}^{(l)}) + \frac{1}{2}\zeta(z)\Omega_p^{(l)}\tilde{\rho}_{12}^{(0)} = G^{(l)}, \quad (\text{B7})$$

$$i\left(\frac{\partial}{\partial t_0} + d_{42}\right)\tilde{\rho}_{42}^{(l)} - \frac{1}{2}\zeta(z)\Omega_c\tilde{\rho}_{43}^{(l)} + \frac{1}{2}\zeta(z)\Omega_s\tilde{\rho}_{12}^{(l)} = H^{(l)}, \quad (\text{B8})$$

$$i\left(\frac{\partial}{\partial t_0} + d_{43}\right)\tilde{\rho}_{43}^{(l)} + \frac{1}{2}\zeta(z)\Omega_s\tilde{\rho}_{13}^{(l)} - \frac{1}{2}\zeta^*(z)\Omega_c^*\tilde{\rho}_{42}^{(l)} - \frac{1}{2}\zeta^*(z)\Omega_p^{*(l)}\tilde{\rho}_{41}^{(0)} = I^{(l)}, \quad (\text{B9})$$

where we have assumed the multiple scale time and position expansions as

$$\frac{\partial}{\partial t} = \frac{\partial}{\partial t_0} + \epsilon \frac{\partial}{\partial t_1}$$

and

$$\frac{\partial}{\partial x} = \frac{\partial}{\partial x_0} + \epsilon \frac{\partial}{\partial x_1} + \epsilon^2 \frac{\partial}{\partial x_2}.$$

We mentioned that this assumption is compatible to that of the formalism extended in [50]. The asymptotic expansion of the Bloch equation can also be written as

$$i\left(\frac{\partial}{\partial x_0} + \frac{1}{n_{\text{eff}c}} \frac{\partial}{\partial t_0}\right)\Omega_p^{(l)} + \kappa_{13}(\tilde{\rho}_{13}^{(l)}) = Q^{(l)}. \quad (\text{B10})$$

In our formalism for linear analyses  $l = 1$ , we seek a solution of the form  $\Omega_p^{(1)} = F \exp(i\phi)$ , where  $\phi = K(\omega)x - \omega t = K(\omega)x_0 - \omega t_0$ ;  $F$  is the yet to be determined probe field envelope that is assumed to be slowly varying variables  $x_2$ ,  $x_1$ , and  $t_1$ . The right-hand side of Eqs. (B1)–(B9) for the various orders can be obtained as  $A^{(1)} = B^{(1)} = C^{(1)} = D^{(1)} = E^{(1)} = F^{(1)} = G^{(1)} = H^{(1)} = I^{(1)} = 0$  and  $Q^{(1)} = 0$ . In the second order we have  $A^{(2)} = C^{(2)} = 0$ ,  $B^{(2)} = \zeta^*(z)\Omega_p^{*(1)}\tilde{\rho}_{31}^{(1)} - \zeta(z)\Omega_p^{(1)}\tilde{\rho}_{13}^{(1)}$ ,  $H^{(2)} = -i\partial\tilde{\rho}_{42}^{(1)}/\partial t_1$  and other elements can be expressed as follows:

$$D^{(2)} = -i\frac{\partial\tilde{\rho}_{21}^{(1)}}{\partial t_1} + \frac{1}{2}\zeta(z)\Omega_p^{(1)}\tilde{\rho}_{23}^{(1)}, \quad (\text{B11})$$

$$E^{(2)} = -i\frac{\partial\tilde{\rho}_{31}^{(1)}}{\partial t_1} - \frac{1}{2}\zeta(z)\Omega_p^{(1)}(\tilde{\rho}_{11}^{(1)} - \tilde{\rho}_{33}^{(1)}), \quad (\text{B12})$$

$$F^{(2)} = -i\frac{\partial\tilde{\rho}_{41}^{(1)}}{\partial t_1} + \frac{1}{2}\zeta(z)\Omega_p^{(1)}\tilde{\rho}_{43}^{(1)}, \quad (\text{B13})$$

$$G^{(2)} = -i\frac{\partial\tilde{\rho}_{32}^{(1)}}{\partial t_1} - \frac{1}{2}\zeta(z)\Omega_p^{(1)}\tilde{\rho}_{12}^{(1)}, \quad (\text{B14})$$

$$I^{(2)} = -i\frac{\partial\tilde{\rho}_{43}^{(1)}}{\partial t_1} + \frac{1}{2}\zeta^*(z)\Omega_p^{*(1)}\tilde{\rho}_{41}^{(1)}, \quad (\text{B15})$$

$$Q^{(2)} = -i\left(\frac{\partial}{\partial x_1} + \frac{1}{n_{\text{eff}c}} \frac{\partial}{\partial t_1}\right)\Omega_p^{(1)}. \quad (\text{B16})$$

By substituting Eqs. (B11)–(B16) into Eqs. (B1)–(B10) and solving these equations in terms of  $\Omega_p^{(2)}$ , it is straightforward to obtain  $\hat{L}\Omega_p^{(2)} = S^{(2)}$ , i.e.,

$$\hat{L}\Omega_p^{(2)} = iZ e^{i\phi} \left( \frac{\partial F}{\partial x_1} + \frac{\partial K(\omega)}{\partial \omega} \frac{\partial F}{\partial t_1} \right), \quad (\text{B17})$$

where the expressions for  $Z$  and  $\hat{L}$  are omitted since they are lengthy. The solvability condition in this order can be readily obtained as follows:

$$\left( \frac{\partial F}{\partial x_1} + \frac{\partial K(\omega)}{\partial \omega} \frac{\partial F}{\partial t_1} \right) = 0. \quad (\text{B18})$$

This expression denotes that the linear surface polariton can be propagated with  $V_g = [\partial K(\omega)/\partial \omega]^{-1}$ ; however, this order does not give any information about the pulse shape of the surface polaritons. As a result, with the first and second order we go to the third order ( $l = 3$ ). In this order the right-hand side of Eqs. (B1)–(B9) can be expressed as follows:  $A^{(3)} = -i\partial\tilde{\rho}_{22}^{(2)}/\partial t_1$ ,  $C^{(3)} = -i\partial\tilde{\rho}_{44}^{(2)}/\partial t_1$ ,  $B^{(3)} = \zeta^*(z)(\Omega_p^{*(2)}\tilde{\rho}_{31}^{(1)} + \Omega_p^{*(1)}\tilde{\rho}_{31}^{(2)}) - \zeta(z)(\Omega_p^{(2)}\tilde{\rho}_{13}^{(1)} + \Omega_p^{(1)}\tilde{\rho}_{13}^{(2)})$ , and  $H^{(3)} = -i\partial\tilde{\rho}_{42}^{(2)}/\partial t_1$  and other coefficients can be written as

$$D^{(3)} = -i\frac{\partial\tilde{\rho}_{21}^{(2)}}{\partial t_1} + \frac{1}{2}\zeta(z)(\Omega_p^{(2)}\tilde{\rho}_{23}^{(1)} + \Omega_p^{(1)}\tilde{\rho}_{23}^{(2)}), \quad (\text{B19})$$

$$E^{(3)} = -i\frac{\partial\tilde{\rho}_{31}^{(2)}}{\partial t_1} - \frac{1}{2}\zeta(z)[\Omega_p^{(2)}(\tilde{\rho}_{11}^{(1)} - \tilde{\rho}_{33}^{(1)}) + \Omega_p^{(1)}(\tilde{\rho}_{11}^{(2)} - \tilde{\rho}_{33}^{(2)})], \quad (\text{B20})$$

$$F^{(3)} = -i\frac{\partial\tilde{\rho}_{41}^{(2)}}{\partial t_1} + \frac{1}{2}\zeta(z)(\Omega_p^{(2)}\tilde{\rho}_{43}^{(1)} + \Omega_p^{(1)}\tilde{\rho}_{43}^{(2)}), \quad (\text{B21})$$

$$G^{(3)} = -i\frac{\partial\tilde{\rho}_{32}^{(2)}}{\partial t_1} - \frac{1}{2}\zeta(z)(\Omega_p^{(2)}\tilde{\rho}_{12}^{(1)} + \Omega_p^{(1)}\tilde{\rho}_{12}^{(2)}), \quad (\text{B22})$$

$$I^{(3)} = -i\frac{\partial\tilde{\rho}_{43}^{(2)}}{\partial t_1} + \frac{1}{2}\zeta^*(z)(\Omega_p^{*(2)}\tilde{\rho}_{41}^{(1)} + \Omega_p^{*(1)}\tilde{\rho}_{41}^{(2)}), \quad (\text{B23})$$

$$Q^{(3)} = -i\left( \frac{\partial}{\partial x_1} + \frac{1}{n_{\text{eff}c}} \frac{\partial}{\partial t_1} \right) \Omega_p^{(2)} - i\frac{\partial}{\partial x_2} \Omega_p^{(1)}. \quad (\text{B24})$$

The substitution of Eqs. (B19)–(B24) into Eqs. (B1)–(B10) and solving the resultant equations in terms of  $\Omega_p^{(3)}$  leads to the operator equations:  $\hat{L}\Omega_p^{(3)} = S^{(3)}$ , i.e.,

$$\hat{L}\Omega_p^{(3)} = Z e^{i\phi} \left( i\frac{\partial F}{\partial x_2} - \frac{K_2}{2} \frac{\partial^2 F}{\partial t_1^2} + W|F|^2 F \right). \quad (\text{B25})$$

The solvability condition of Eq. (B25) (i.e.,  $\Omega_p^{(3)} = 0$ ) gives Eq. (48).

### APPENDIX C: COEFFICIENTS OF THE FIRST-ORDER PERTURBATIVE SOLUTION

The coefficients of the first-order perturbative solution can be expressed as follows:

$$a_{21}^{(1)} = \frac{[(d_{31} + \omega)D_c^* - |\zeta(z)\Omega_s|^2(d_{24} + \omega)]\tilde{\rho}_{32}^{*(0)} + D_p\tilde{\rho}_{41}^{*(0)} + \zeta(z)\Omega_c[D_c - |\zeta(z)\Omega_s|^2(\tilde{\rho}_{11}^{(0)} - \tilde{\rho}_{33}^{(0)})]}{(d_{13} - d_{42})\{D_{cs} + (d_{42} - d_{13})[D_c(d_{12} + \omega) - |\zeta(z)\Omega_s|^2(d_{43} + \omega)]\}}, \quad (\text{C1})$$

$$a_{42}^{(1)} = \frac{\zeta(z)\Omega_s D_{32}\tilde{\rho}_{32}^{*(0)} - \zeta(z)\Omega_c D_{41}\tilde{\rho}_{41}^{*(0)} + \zeta(z)^2\Omega_c\Omega_s(d_{43} - d_{12})(\tilde{\rho}_{11}^{(0)} - \tilde{\rho}_{33}^{(0)})}{(d_{13} - d_{42})\{D_{cs} + (d_{42} - d_{13})[D_c(d_{12} + \omega) - |\zeta(z)\Omega_s|^2(d_{43} + \omega)]\}}, \quad (\text{C2})$$

$$a_{43}^{(1)} = \frac{D_p\tilde{\rho}_{32}^{(0)} + [D_s(d_{13} + \omega) - D_c(d_{42} + \omega)]\tilde{\rho}_{41}^{(0)} + \zeta(z)\Omega_s X(\tilde{\rho}_{11}^{(0)} - \tilde{\rho}_{33}^{(0)})}{(d_{13} - d_{42})\{D_{cs} + (d_{42} - d_{13})[D_c(d_{12} + \omega) - |\zeta(z)\Omega_s|^2(d_{43} + \omega)]\}}, \quad (\text{C3})$$

where

$$\begin{aligned} D_p &= \zeta(z)^2\Omega_c\Omega_s(d_{24} - d_{31}), \\ X &= |\zeta(z)\Omega_c|^2 - |\zeta(z)\Omega_s|^2 + (d_{12} + \omega)(d_{42} + \omega), \\ D_{32} &= |\zeta(z)\Omega_c|^2 - |\zeta(z)\Omega_s|^2 + (d_{13} + \omega)(d_{43} + \omega), \\ D_{41} &= |\zeta(z)\Omega_c|^2 - |\zeta(z)\Omega_s|^2 + (d_{12} + \omega)(d_{13} + \omega). \end{aligned} \quad (\text{C4})$$

**APPENDIX D: COEFFICIENTS OF THE SECOND-ORDER PERTURBATIVE SOLUTION**

The explicit forms of the density matrix coefficients ( $a_{jl}^{(2)}$ ) in the second order read

$$a_{22}^{(2)} = \frac{J_1 J_2 (a_{31}^{(1)} - a_{31}^{*(1)}) + \gamma_{43} J_2 X_{41} \zeta(z) \Omega_s (a_{43}^{(1)} - a_{43}^{*(1)}) + X_{32} \zeta^*(z) \Omega_c J_3 (a_{21}^{(1)} - a_{21}^{*(1)})}{\Gamma_4 \gamma_{31} |\zeta(z) \Omega_c|^2 X_{32} + X_{14} |\zeta(z) \Omega_s|^2 [\gamma_{32} \gamma_{43} - 2i X_{32} (\gamma_{31} + \gamma_{32}) |\zeta(z) \Omega_c|^2]}, \quad (\text{D1})$$

$$a_{33}^{(2)} = \frac{J_1 X_{32} |\zeta(z) \Omega_c|^2 (a_{31}^{(1)} - a_{31}^{*(1)}) - X_{41} X_{32} g_{43} |\zeta(z)|^2 \zeta(z) \Omega_s \Omega_c [\Omega_c (a_{21}^{(1)} - a_{21}^{*(1)}) - \Omega_s g_{43} (a_{43}^{(1)} - a_{43}^{*(1)})]}{\Gamma_4 \gamma_{31} |\zeta(z) \Omega_c|^2 X_{32} + X_{14} |\zeta(z) \Omega_s|^2 [\gamma_{32} \gamma_{43} - 2i X_{32} (\gamma_{31} + \gamma_{32}) |\zeta(z) \Omega_c|^2]}, \quad (\text{D2})$$

$$a_{44}^{(2)} = \frac{X_{14} J_2 |\zeta(z) \Omega_s|^2 (a_{31}^{(1)} - a_{31}^{*(1)}) + X_{41} X_{32} g_{43} |\zeta(z)|^2 \zeta(z) \Omega_s \Omega_c [\Omega_c (a_{21}^{(1)} - a_{21}^{*(1)}) - \Omega_s g_{43} (a_{43}^{(1)} - a_{43}^{*(1)})]}{\Gamma_4 \gamma_{31} |\zeta(z) \Omega_c|^2 X_{32} + X_{14} |\zeta(z) \Omega_s|^2 [\gamma_{32} \gamma_{43} - 2i X_{32} (\gamma_{31} + \gamma_{32}) |\zeta(z) \Omega_c|^2]}, \quad (\text{D3})$$

where

$$J_1 = \Gamma_{44} - 2i X_{41} |\zeta(z) \Omega_s|^2, \quad J_2 = \gamma_{32} - 2i X_{32} |\zeta(z) \Omega_c|^2, \quad (\text{D4})$$

$$J_3 = X_{32} \zeta(z) \Omega_c [\gamma_{32} \Gamma_{44} - i X_{14} (2\gamma_{31} + \gamma_{43}) |\zeta(z) \Omega_s|^2].$$

The other matrix elements can be directly observed with the second-order perturbation of the Bloch equations as follows:

$$a_{41}^{(2)} = \frac{1}{2d_{41}} [\zeta(z) \Omega_s (a_{44}^{(2)} - a_{11}^{(2)}) + \zeta(z) \Omega_p a_{43}^{(1)}],$$

$$a_{32}^{(2)} = \frac{1}{2d_{32}} [\zeta(z) \Omega_c (a_{33}^{(2)} - a_{22}^{(2)}) - \zeta^*(z) \Omega_s^* a_{12}^{(1)}]. \quad (\text{D5})$$

Moreover, other matrix elements in the second-order approximation can be obtained from the matrix

$$\begin{pmatrix} \tilde{\rho}_{21}^{(2)} \\ \tilde{\rho}_{31}^{(2)} \\ \tilde{\rho}_{42}^{(2)} \\ \tilde{\rho}_{43}^{(2)} \end{pmatrix} = \begin{pmatrix} \omega - d_{21} & \frac{\zeta^*(z) \Omega_c^*}{2} & \frac{-\zeta(z) \Omega_s}{2} & 0 \\ \frac{\zeta(z) \Omega_c}{2} & \omega - d_{31} & 0 & \frac{-\zeta(z) \Omega_s}{2} \\ \frac{-\zeta^*(z) \Omega_s^*}{2} & 0 & \omega - d_{42}^* & \frac{\zeta^*(z) \Omega_c^*}{2} \\ 0 & \frac{-\zeta^*(z) \Omega_s^*}{2} & \frac{\zeta(z) \Omega_c}{2} & \omega - d_{43}^* \end{pmatrix}^{-1} \begin{pmatrix} -i \frac{\partial}{\partial t_1} \tilde{\rho}_{21}^{(1)} \\ -i \frac{\partial}{\partial t_1} \tilde{\rho}_{31}^{(1)} \\ -i \frac{\partial}{\partial t_1} \tilde{\rho}_{42}^{(1)} \\ -i \frac{\partial}{\partial t_1} \tilde{\rho}_{43}^{(1)} \end{pmatrix}. \quad (\text{D6})$$

**APPENDIX E: EXPLICIT SOLUTION OF THE HIGHER-ORDER SP AKHMEDIEV BREATHERS SOLUTION**

The coefficient appearing in Eq. (71) can be obtained by the following expressions:

$$m_{12}^* = \frac{2e^{is'}}{D_1} \{\alpha_1 [\cos(2\mathcal{A}_r) - \cosh(2\mathcal{A}_i)] + \alpha_2 [\cos(2\mathcal{B}_r) + \cosh(2\mathcal{B}_i)] \sinh(\mathcal{C}) - 4i\mathcal{J} \cosh(\mathcal{F})\}, \quad (\text{E1})$$

$$s_{12} = \frac{2e^{is'}}{D_1} \{\alpha_3 [\cosh(2\mathcal{A}_i) - \cos(2\mathcal{A}_r)] + \alpha_4 [\cos(2\mathcal{B}_r) + \cosh(2\mathcal{B}_i)] \sinh(\mathcal{F}^*) - 4i\mathcal{J} \cosh(\mathcal{C}^*)\}, \quad (\text{E2})$$

where  $\mathcal{J} = \sinh(\mathcal{A}) \cosh(\mathcal{C}^*)$  with

$$\alpha_1 = \nu_2 - \nu_1 + i(l_1 - l_2), \quad \alpha_2 = \nu_1 - \nu_2 + i(l_1 - l_2),$$

$$\alpha_3 = \nu_2 - \nu_1 + i(l_1 + l_2), \quad \alpha_4 = \nu_2 - \nu_1 + i(l_2 - l_1). \quad (\text{E3})$$

Moreover, in obtaining the above formula, we assumed

$$\begin{aligned} \mathcal{A}_r &= \xi_r + (\Omega_r \tau / \tau_0 + \vartheta_i) / 2 - \pi / 4, & \mathcal{A}_i &= \xi_i + (\Omega_i \tau / \tau_0 - \vartheta_r) / 2, \\ \mathcal{C}_r &= \xi'_r + (\Omega'_r \tau / \tau_0 + \vartheta'_i) / 2 - \pi / 4, & \mathcal{C}_i &= \xi'_i + (\Omega'_i \tau / \tau_0 - \xi'_r) / 2, \\ \mathcal{B}_r &= -(\xi_r + \pi / 4) + (\Omega_r \tau / \tau_0 + \vartheta_i) / 2, & \mathcal{B}_i &= -\xi_i + (\Omega_i \tau / \tau_0 - \vartheta_r) / 2, \\ \mathcal{F}_r &= -(\xi'_r + \pi / 4) + (\Omega'_r \tau / \tau_0 + \vartheta'_i) / 2, & \mathcal{F}_i &= -\xi'_i + (\Omega'_i \tau / \tau_0 - \vartheta'_r) / 2, \\ D_1 &= \cosh(2\mathcal{A}_i) - \cos(2\mathcal{A}_r) + \cosh(2\mathcal{B}_i) + \cos(2\mathcal{B}_r). \end{aligned} \quad (\text{E4})$$

[1] D. R. Solli, C. Ropers, P. Koonath, and B. Jalali, *Nature (London)* **450**, 1054 (2007).

[2] J. M. Dudley, F. Dias, M. Erkintalo, and G. Genty, *Nat. Photon.* **8**, 755 (2014).

[3] N. Akhmediev, B. Kibler, F. Baronio, M. Belić, W.-P. Zhong, Y. Zhang, W. Chang, J. M. Soto-Crespo, P. Vouzas, and P. Grellu, *Others. J. Opt.* **18**, 063001 (2016).

- [4] N. Akhmediev, J. M. Soto-Crespo, and A. Ankiewicz, *Phys. Rev. A* **80**, 043818 (2009).
- [5] F. Baronio, S. Chen, P. Grelu, S. Wabnitz, and M. Conforti, *Phys. Rev. A* **91**, 033804 (2015).
- [6] D. H. Peregrine, *J. Aust. Math. Soc. Ser. B* **25**, 16 (1983).
- [7] A. Montana, U. Bortolozzo, S. Residori, and F. T. Arecchi, *Phys. Rev. Lett.* **103**, 173901 (2009).
- [8] D. Pierangeli, F. Di Mei, C. Conti, A. J. Agrat, and E. DelRe, *Phys. Rev. Lett.* **115**, 093901 (2015).
- [9] Y. V. Bludov, V. V. Konotop, and N. Akhmediev, *Phys. Rev. A* **80**, 033610 (2009).
- [10] S. Birkholz, E. T. J. Nibbering, C. Brée, S. Skupin, A. Demircan, G. Genty, and G. Steinmeyer, *Phys. Rev. Lett.* **111**, 243903 (2013).
- [11] J. M. Dudley, G. Genty, F. Dias, B. Kibler, and N. Akhmediev, *Opt. Express* **17**, 21497 (2009).
- [12] L. Wang, J.-H. Zhang, Z.-Q. Wang, C. Liu, M. Li, F.-H. Qi, and R. Guo, *Phys. Rev. E* **93**, 012214 (2016).
- [13] A. Ankiewicz and N. Akhmediev, *Phys. Rev. E* **96**, 012219 (2017).
- [14] L. Liu, B. Tian, H.-P. Chai, and Y.-Q. Yuan, *Phys. Rev. E* **95**, 032202 (2017).
- [15] Y. Ohta and J. Yang, *Phys. Rev. E* **86**, 036604 (2012).
- [16] A. Ankiewicz, J. M. Soto-Crespo, and N. Akhmediev, *Phys. Rev. E* **81**, 046602 (2010).
- [17] Y. Tao and J. He, *Phys. Rev. E* **85**, 026601 (2012).
- [18] B. Kibler, J. Fatome, C. Finot, G. Millot, F. Dias, G. Genty, N. Akhmediev, and J. M. Dudley, *Nat. Phys.* **6**, 790 (2010).
- [19] A. Zaviyalov, O. Egorov, R. Iliew, and F. Lederer, *Phys. Rev. A* **85**, 013828 (2012).
- [20] J. Zamora-Munt, B. Garbin, S. Barland, M. Giudici, J. R. R. Leite, C. Masoller, and J. R. Tredicce, *Phys. Rev. A* **87**, 035802 (2013).
- [21] D. Buccoliero, H. Steffensen, H. Ebendorff-Heidepriem, T. M. Monro, and O. Bang, *Opt. Express* **19**, 17973 (2011).
- [22] K. Hammani and F. Christophe, *Opt. Fiber Tech.* **18**, 93 (2012).
- [23] F. Baronio, M. Conforti, A. Degasperis, and S. Lombardo, *Phys. Rev. Lett.* **111**, 114101 (2013).
- [24] D. Majus, V. Jukna, G. Valiulis, D. Faccio, and A. Dubietis, *Phys. Rev. A* **83**, 025802 (2011).
- [25] C. N. Kumar, R. Gupta, A. Goyal, S. Loomba, T. S. Raju, and P. K. Panigrahi, *Phys. Rev. A* **86**, 025802 (2012).
- [26] G. Yang, L. Li, and S. Jia, *Phys. Rev. E* **85**, 046608 (2012).
- [27] A. Coillet, J. M. Dudley, G. Genty, L. Larger, and Y. K. Chembo, *Phys. Rev. A* **89**, 013835 (2014).
- [28] S. Toenger, T. Godin, C. Billet, F. Dias, M. Erkintalo, G. Genty, and J. M. Dudley, *Sci. Rep.* **5**, 10380 (2015).
- [29] S. Chen, Y. Ye, F. Baronio, Y. Liu, X.-M. Cai, and P. Grelu, *Opt. Express* **25**, 29687 (2017).
- [30] A. Tikan, C. Billet, G. El, A. Tovbis, M. Bertola, T. Sylvestre, F. Gustave, S. Randoux, G. Genty, P. Suret, and J. M. Dudley, *Phys. Rev. Lett.* **119**, 033901 (2017).
- [31] Zh. Bai and G. Huang, *Opt. Express* **24**, 4442 (2016).
- [32] J. Liu, C. Hang, and G. Huang, *Phys. Rev. A* **93**, 063836 (2016).
- [33] S. A. Moiseev, A. A. Kamli, and B. C. Sanders, *Phys. Rev. A* **81**, 033839 (2010).
- [34] Y. V. Bludov, D. A. Smirnova, Y. S. Kivshar, N. M. R. Peres, and M. I. Vasilevskiy, *Phys. Rev. B* **89**, 035406 (2014).
- [35] C. Tan and G. Huang, *Phys. Rev. A* **91**, 023803 (2015).
- [36] S. Asgarneshad-Zorgabad, R. Sadighi-Bonabi, and C. Hang, *J. Opt. Soc. Am. B* **34**, 1787 (2017).
- [37] J. Sheng, X. Yang, U. Khadka, and M. Xiao, *Opt. Express* **19**, 17059 (2011).
- [38] J. A. Schuller, E. S. Barnard, W. Cai, Y. C. Jun, J. S. White, and M. L. Brongersma, *Nat. Mater.* **9**, 193 (2010).
- [39] Our work deals with the coupler free SP excitation. The surface plasmon polariton (SPP) excitation in a coupler free planar waveguide is investigated in C. Du, Q. Jing, and Z. Hu, *Phys. Rev. A* **91**, 013817 (2015).
- [40] The proposed design is very different from the coupler free scheme represented in [36]. (i) The complexity of the vapor cell MOT design and inducing unidirectional motion to the atoms requires a high technologic optical device; however, in this scheme, the narrow EIT position is achieved with proper adjustment of the laser fields, which is easier to observe in the experiment. (ii) The field concentration and linear properties of the present model are more efficient than that of [36]. (iii) In the mentioned reference, only the excitation and stability of SP solitons is discussed.
- [41] H. Raether, *Surface Plasmons on Smooth and Rough Surfaces and on Gratings* (Springer, Berlin, 1988).
- [42] M. E. Crenshaw and C. M. Bowden, *Phys. Rev. A* **53**, 1139 (1996).
- [43] By taking the realistic parameters of the  $^{87}\text{Rb}$  atomic medium, one obtains  $T \ll 0.1$  K. See, e.g., L. Li and G. Huang, *Phys. Rev. A* **82**, 023809 (2010).
- [44] S. A. Maier, *Plasmonics: Fundamentals and Applications* (Springer, Berlin, 2007).
- [45] V. M. Shalaev, *Nat. Photon.* **1**, 41 (2007).
- [46] S. Xiao, U. K. Chettiar, A. V. Kildishev, A. P. Drachev, and V. M. Shalaev, *Opt. Lett.* **34**, 3478 (2009).
- [47] D. Steck,  $^{87}\text{Rb}$  D Line Data, <http://steck.us/alkalidata>.
- [48] J. Sheng, X. Yang, H. Wu, and M. Xiao, *Phys. Rev. A* **84**, 053820 (2011).
- [49] Our analysis is based on two assumptions. (i) In the presented work,  $\omega_{\text{EIT}}$  is the center of the EIT window and is different from  $\omega$  which is the perturbation of the SP's wave. (ii) Here  $\omega_{\text{EIT}}$  is chosen for lossless propagation and as a result the optical properties such as group velocity and GVD are obtained by frequency deviation from this EIT window.
- [50] For application of the multiscale variable method to the partial differential equations, see, e.g., J. Kevorkian and J. D. Cole, *Multiple-Scale Expansions for Partial Differential Equations* (Springer, Berlin, 1996).
- [51] G. Huang, L. Deng, and M. G. Payne, *Phys. Rev. E* **72**, 016617 (2005).
- [52] J. D. Jackson, *Classical Electrodynamics*, 3rd ed. (Wiley Online Library, New York, 1999).
- [53] A. Chabchoub, N. P. Hoffmann, and N. Akhmediev, *Phys. Rev. Lett* **106**, 204502 (2011).
- [54] A. Slunyaev, E. Pelinovsky, A. Sergeeva, A. Chabchoub, N. P. Hoffmann, M. Onorato, and N. Akhmediev, *Phys. Rev. E* **88**, 012909 (2013).
- [55] A. Chabchoub, N. P. Hoffmann, M. Onorato, and N. Akhmediev, *Phys. Rev. X* **2**, 011015 (2012).
- [56] N. Akhmediev, J. M. Soto-Crespo, and A. Ankiewicz, *Phys. Lett. A* **373**, 2137 (2009).